enzymes have been prime therapies used to lower the Aβ level [59-61]. γ-Secretase inhibitors such as LY450139 reduce the production of both Aβ40 and Aβ42 [62], while γ-secretase modulators such as Flurizan™ lower Aβ42 production by selectively modulating, but not inhibiting, γ-secretase activity, to shift the cleavage of APP away from Aβ42 production [63]. At present, LY450139 and Flurizan™ are being evaluated in human clinical Phase II and III trials, respectively.

Preventing the formation and deposition of Aβ fibrils represents another promising approach to developing disease-modifying drugs. Alzhemed™, a glycosaminoglycan mimic that binds to soluble Aβ, is one of the most advanced drugs that inhibits Aβ fibrilization, and is currently under clinical evaluation in Phase III trials [64].

As an alternative strategy that targets Aβ directly, antibody-mediated Aβ clearance or removal from the brain also has potential for reducing Aβ accumulation in the brain. Active immunization with the Aβ immuno-conjugate ACC-001, which is composed of an N-terminal fragment of Aβ and a carrier protein, and passive immunization with the humanized monoclonal antibody AAB-001 are now undergoing clinical trials [65].

Collectively, several drug candidates designed to modify amyloidogenic processes in the early stages of Alzheimer's amyloid pathology are currently under clinical evaluation. For the appropriate evaluation of drug efficacy, there is an essential need for biomarkers that indicate whether drugs are actually altering the underlying degenerative process. In addition, appropriate biomarkers for the early diagnosis of AD are also required, because anti-amyloid therapy should be started as early as possible after the initiation of amyloid pathology to obtain an optimum therapeutic effect and to delay or halt the clinical outcomes.

4. AMYLOID IMAGING

Since AD is a progressive neurodegenerative disorder leading to the death of neurons that cannot be replaced once lost, an early diagnosis is critical for physicians, patients and their families to make early social, legal, and medical decisions about treatment and care. Early treatment with even current medications, starting before neurodegeneration becomes too severe and widespread, may provide greater benefits over the long term [66,67]. Moreover, early diagnosis and treatment of AD are expected to contribute substantially to social and financial savings. Consequently, a considerable effort has been made in the last decade to identify reliable biomarkers of AD for disease detection at an early stage [18,68].

At present, clinical diagnosis of AD is generally performed by evaluation of the progressive impairment of cognitive functions and exclusion of other causes of dementia. A definitive diagnosis of AD can only be made by postmortem observation of NPs and NFTs in brain sections; this is regarded as the gold standard [69,70]. This mean that, according to current clinical diagnostic criteria, AD can not be diagnosed before the disease has progressed so far that clinical outcomes have appeared. Recent studies have demonstrated that PET imaging of glucose metabolism and CSF biomarkers (total tau, phosphorylated tau, and Aβ42) show preliminary promise for the identification of AD traits [68,71]. Both methods indicate a high predictive value for the identification of preclinical AD in patients with mild cognitive impairment (MCI), which is suggestive of the earliest symptomatic stage of AD but is insufficient to fulfill traditional diagnostic criteria for AD [72]. However, postmortem studies have revealed that some cognitively intact individuals and many patients with MCI already carry a heavy burden of AD-like neuropathology [73-75]. The pathogenic processes, especially the formation of NPs, are estimated to start a few decades before clinical symptoms become evident (Fig. (2)). Considering this fact along with the amyloid cascade hypothesis, Aβ deposits in the brain are a reasonable and promising biomarker for the early diagnosis of AD.

To detect Aβ burden in the brain, much attention has been directed toward amyloid imaging, which enables the spatial distribution and degree of deposition of Aβ in the brain to be visualized non-invasively using a ligand that binds to Aβ fibrils. This *in vivo* imaging measurement would have great value as a diagnostic marker for identifying individuals with incipient AD in the MCI stage, and even those in the presymptomatic phase of the disease. Amyloid imaging would allow us to investigate the pathogenic role of Aβ in AD pathology by following and relating directly the pathological progression and cognitive decline in the same individuals over time.

In addition, amyloid imaging is expected to serve as a useful tool for the clinical assessment of disease-modifying therapeutics targeting the Aβ pathway, making it possible to evaluate whether the level of Aβ deposits in the brain is lowered by the drug; namely, whether the drugs actually exert their action against their targets [22,76,77]. Such *in vivo* evaluation of drug influences on disease targets would provide convincing proof of the mechanism. Furthermore, selection of appropriate subjects who have Aβ deposits in their brains, but intact cognition, using amyloid imaging, would be a rational strategy for clinical trials of such disease-modifying therapeutics. Measurement of Aβ deposition by amyloid imaging may be more reliable than measurement of standard clinical or cognitive outcomes in large clinical trials, thereby increasing the power to detect a small effect and reducing sample size.

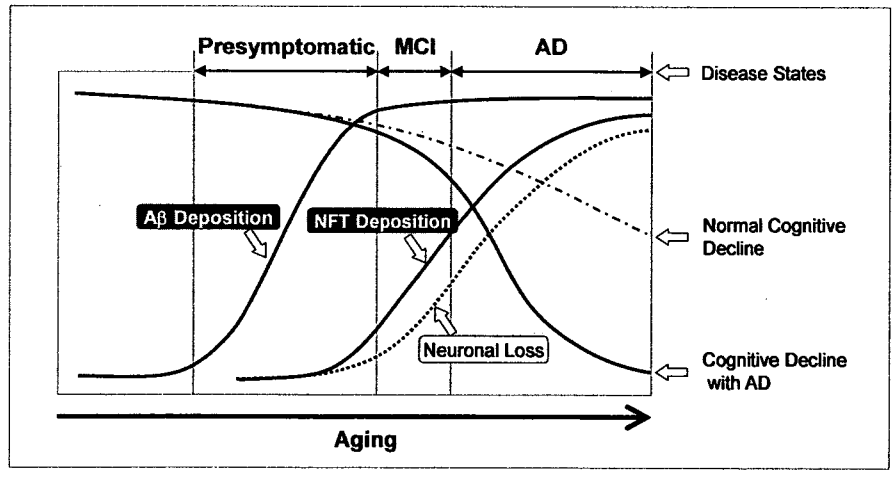

Fig. (2). Hypothetical model of the neuropathological progression (Aβ and NFT depositions) and clinical outcomes in Alzheimer's disease.

Development of amyloid imaging agents, including probes for PET, SPECT, Magnetic Resonance Imaging [78-80], and near-infrared fluorescence imaging [81], have advanced rapidly during the last decade. Among these, PET radioligands have been the most extensively studied, and a significant number of candidates have been reported to date. Some of these have proceeded to exploratory clinical evaluations and promising results have been achieved in amyloid imaging studies.

5. AMYLOID IMAGING AGENTS

5.1. Requirements for Amyloid Imaging Agents

In general, development of PET radioligands starts with finding a "seed" compound, which binds to the target molecule. The chemical structure is then optimized to have appropriate features for imaging the target. With regard to amyloid imaging, the radioligand requires several criteria for optimization, including that it shows: high binding affinity for Aβ fibrils; high blood-brain barrier (BBB) permeability with appropriate lipophilicity; and excellent brain pharmacokinetics with rapid brain uptake and fast clearance from the normal brain without non-specific binding.

The binding affinity required for radioligands is generally considered in relation to the total concentration of the target molecule. The concentrations of Aβ in the AD brain have been reported to be 1-10 μM [82], and these levels are considerably higher than those of typical neuroreceptors or transporters (1-200 nM) [83]. Therefore, the requisite binding affinities (Kd; the equilibrium dissociation constant) for amyloid imaging agents have been set as below 20 nM [84], which is relatively higher than those of neuroreceptors or transporters in the range between 10 pM and 1 nM [83]. As an alternative indicator, inhibition constant (Ki) is also often used for evaluating binding affinities due to its utility in the efficient screening of a number of non-radiolabeled candidates; this value is required to achieve the same level as the Kd.

Showing a high BBB permeability via passive diffusion, a radioligand for amyloid imaging should be a small molecule with a molecular weight (MW) of less than 400-500 [85]. In addition, the radioligand should be lipophilic enough to cross the BBB easily, but not so lipophilic as to cause unacceptable binding to plasma proteins and non-specific binding to normal brain tissue. A parabolic relationship has been demonstrated between radiotracer brain uptake and its Log P value, an octanol-water partition coefficient used as a parameter of lipophilicity, showing the uptake peak between a Log P of 2 and 3 [86,87]. The appropriate Log P value for brain entry has been suggested to be in the range between 1 and 3 [88].

Because of the short half-lives of positron emitters (^{11}C, 20.4 min; ^{18}F, 109.8 min), intravenously injected radioligand should be incorporated rapidly into the brain and, after reaching the peak level of uptake, non-specific bound or free radioligand should be cleared fast in the half-life time equal to or less than that of the radioactive decay of the radionuclide [27,89]. For this purpose, binding affinity, MW, and lipophilicity of radioligands are comprehensively optimized to afford desirable pharmacokinetic properties leading to adequate images with a high signal-to-noise ratio suitable for quantitative analysis of ligand binding potency.

5.2. Biomolecules

Some biomolecules such as antibodies or Aβ peptide itself were explored in the search of amyloid imaging agents, because they bind specifically to Aβ amyloid and plaques *in vitro* [90-94]. However, these molecules do not possess the appropriate properties for brain amyloid imaging in *in vivo* studies. One of the most serious problems is their low BBB permeability due to their large MW. Although many attempts have been made to improve their BBB permeability (brain uptake) by modifying their structure or applying a drug delivery system, no promising results have yet been achieved. Therefore, over the past decade, an alternative approach for developing amyloid imaging agents, based on small organic compounds, has been taken.

5.3. Congo Red Analogues

Congo red (CR) is an organic dye molecule widely used for the histological staining of amyloid especially in postmortem pathological studies of AD. Klunk and coworkers evaluated quantitatively CR binding to amyloid-like proteins with a β-sheet conformation [95]. They speculated that the key structural feature of CR is the two acidic functional groups and the space between them. Since CR possesses low lipophilicity (Log P = -0.18) owing to two highly charged amino-naphthalene sulfonic acid groups in the structure, Klunk and coworkers investigated the binding potential of Chrysamine G (CG), a lipophilic analogue of CR, which also has two acidic functional groups with the same amount of space between them as seen in CR.

CG showed high binding affinity to synthetic Aβ aggregates (Ki = 2.7 nM), and total binding of [^{14}C]CG to homogenates of AD brains was nearly three times as high as that of age-matched control brains [27,96,97]. However, brain uptake of [^{14}C]CG in mice was limited. Thus, considerable efforts to develop CG derivatives with high BBB permeability were expended through modifying the structure to afford a low MW and relatively high lipophilicity, resulting in a new series of CG analogues (**1-8**) with a new pharmacophore, bis-styryl benzene (styrylbenzene), indicated as Framework A in Fig. (**4**).

Methoxy-X04 (**8**; Me-X04), an optimized CG derivative, has a lower MW (344), lacking the carboxylic acid groups, is moderately lipophilic (Log P = 2.6), and exhibits selective binding to Aβ plaques in postmortem AD brain sections and PS1/APP Tg mouse brain [27,98]. Interestingly, removing the carboxylic acid groups had little effect on the binding affinity for Aβ aggregates and Aβ plaques, indicating that the acidic functional group is not a predominant factor in the binding mechanism. Moreover, removal of the carboxylic acid groups leaving only the weakly acidic phenols resulted in a neutral form of Me-X04 at physiologic pH (pKa = 10.8), and thereby, the brain uptake of [^{11}C]Me-X04 was shown to be 7-fold higher than that of the related carboxylic acid derivative Me-X34 (**7**) [98]. Nevertheless, the level of brain uptake of the optimized compound was still insufficient for using in human PET studies.

The styrylbenzene framework was also used by other researchers for the development of amyloid imaging agents such as ISB, IMSB, and so on [99-101]. Although [^{125}I]ISB (**10**) and [^{125}I]IMSB (**11**) showed high binding affinity to Aβ aggregates, their BBB permeabilities were very low, probably due to their carboxylic acid groups. If the carboxylic acid groups were removed from ISB and IMSB, the brain uptake of the resultant derivatives would be expected to increase, but not to exceed the level of Me-X04 uptake, because of their relatively high MW.

Since the framework of styrylbenzene is so rigid that further optimization of the derivatives is limited, recent research has shifted to the usage of different types of molecular framework for developing amyloid imaging agents.

5.4. Thioflavin-T Analogues

Thioflavin T (ThT) and Thioflavin S (ThS) are other organic dyes often used for histopathological staining of amyloid plaques (Fig. (**3**)). Although ThS is more widely used in *in vitro* histological staining studies, ThT is a more attractive seed compound for developing amyloid imaging agents, because of its relatively low MW and well-defined chemical structure [102]. However, ThT contains a positively charged benzothiazolium unit, whose ionic charge is unfavorable for brain uptake. Therefore, the development of amyloid imaging agents based on ThT requires chemical modification of the charged structure to generate a neutral form.

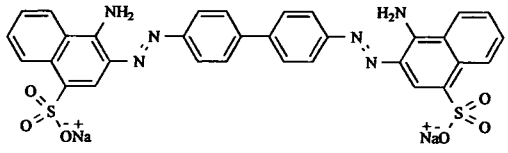

Congo-Red (CR)

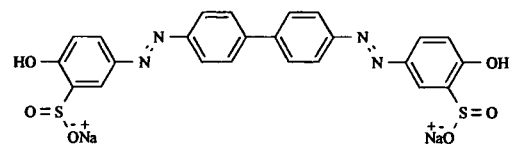

Chrysamine G (CG)

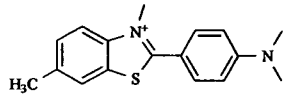

Thioflavin (ThT)

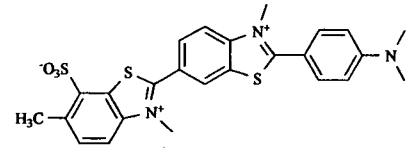

Thioflavin S (ThS), major component

Fig. (3). Organic dye molecules widely used for the histological staining of amyloid.

Klunk and co-coworkers developed a series of neutral ThT derivatives (**13-25**, **30-32**) containing uncharged benzothiazole instead of benzothiazolium for PET imaging [84,103-105]. That is, the molecular framework in the derivatives can be represented as Framework B in Fig. (**4**), where X and Y are "S" and "N", respectively. They systematically evaluated the binding affinities and lipophilicities of the derivatives, and investigated the relationship between the lipophilicity and brain entry or clearance of the derivatives in detail [84]. As a result, all of the neutral derivatives showed higher binding affinities (Ki: 2-64 nM) for Aβ40 aggregates than the charged parent compound, ThT (Ki: 580 nM). Additionally, an interesting correlation was observed between log P_{C18} and the clearance as expressed by the 2 min-to-30 min ratio, indicating that the least lipophilic compounds tended to be cleared from the brain the fastest, while the most lipophilic ones were retained for over 30 min [84]. Based on the brain clearance property, compound **20** (PIB), which showed rapid clearance from normal mouse (2 min-to-30 min ratio = 11.6) and baboon brain, was finally selected as a promising candidate for further biological evaluation. An *in vitro* binding study using [^{3}H]PIB and AD brain homogenates indicated a high binding affinity with Kd value of 2.5 nM [106].

Kung and co-workers also independently developed 2-arylbenzothiazole derivatives as neutral ThT derivatives (**35**, TZDM; **36**, TZPI) for SPECT imaging [100]. These derivatives showed specific binding to Aβ40 and Aβ42 aggregates at sub-nanomolar concentrations. Using [^{125}I]TZDM and [^{125}I]IMSB in a competitive binding assay, these authors clearly demonstrated that there are distinctive and mutually exclusive binding sites on Aβ40 and Aβ42 aggregates for 2-arylbenzothiazole derivatives and styrylbenzene derivatives. Kung and co-workers have continued to develop a variety of ThT derivatives containing benzoxazole (**37**, IBOX) [107], benzofuran (**47-54**) [108,109] or imidazopyridine (**100-104**), in the place of benzothiazolium. Among them, a benzofuran derivative [^{11}C]**50** showed potential for *in vivo* amyloid imaging: high binding affinity (Ki: 0.7 nM) for Aβ and good brain clearance (2 min-to-30 min ratio = 13.6). An imidazopyridine derivative [^{125}I]**100** known as IMPY also demonstrated desirable characteristics for *in vivo* imaging of Aβ plaques [110-114].

As related F-18-labeled compounds, 2-(4-fluorophenyl)benzothiazole derivatives (**33**, **34**) [115,116] and ThT derivatives containing benzothiophene (**38-46**) [117] or imidazopyridine (**105-108**) [118,119] instead of benzothiazolium were also reported by other research groups. The benzothiophene derivatives exhibited excellent binding affinities for Aβ aggregates (Ki: 0.2-4.3 nM) and high initial brain uptake, but very slow clearances from normal brain tissue relative to PIB and **50**. However, their slow clearances would be improved by introducing a hydroxy group into the benzene ring of benzothiophene to reduce their lipophilicities, as in the case of PIB and **50**. For F-18-labeled IMPY analogues ([^{18}F]**105**, [^{18}F]**106**, [^{18}F]**108**), PET studies of brain pharmacokinetics in mice and rhesus monkeys showed moderately favorable profiles; however, further improvements are needed to reduce radioactive metabolites and/or increase binding affinity.

5.5. Stilbene and Related Derivatives

Stilbene, represented as Framework C in Fig. (**4**), where X is "C", is a simple but potent pharmacophore belonging to Aβ binding ligands that were found by Kung and co-workers in a search for a new Aβ probe [120,121]. While the stilbene skeleton is a partial structure of styrylbenzene, an *in vitro* binding assay revealed that the binding affinities of stilbene derivatives toward styrylbenzene binding sites were very low. By contrast, stilbene derivatives showed high binding affinities to the binding sites of TZDM (**35**), a ThT derivative, especially in the case of aromatic rings containing an electron-donating group, such as *p*-amino, *p*-methoxy, or *p*-hydroxy groups [120]. Consequently, a series of simple stilbene derivatives with 4-amino and 4'-hydroxy substitution groups (**58-63**) were screened as possible PET imaging agents [122]. Although all of the stilbenes displayed high binding affinities (Ki: 1-6 nM), compound **61** (SB-13) was selected as a lead compound for C-11 labeling and further biological evaluation because of its moderate lipophilicity. As expected, [^{11}C]SB-13 showed very good brain penetration and clearance from normal rat brain after i.v. injection. In addition, *in vitro* autoradiography demonstrated specific binding of [^{11}C/^{3}H]SB-13 to Aβ deposits in the tissue sections from transgenic AD model mouse brain and AD brain [114]. [^{3}H]SB-13 displayed high-affinity binding to AD brain homogenates with a Kd value of 2.4 nM. These results suggested that simple stilbene derivatives like [^{11}C]SB-13 might have potential for visualizing Aβ deposits in the brain using PET.

Kung and co-workers then designed and synthesized stilbene derivatives (**69**, **71**, **73**) containing a 2-fluoromethylpropan-1-ol structure aiming at F-18-labeled amyloid imaging agents [123]. These compounds exhibited high binding affinities in a competitive binding assay using [^{125}I]IMPY and AD brain homogenates. Biological evaluations using their F-18-labeled compounds clarified that [^{18}F]**73** ([^{18}F]FMAPO) shows the most preferable features: excellent brain penetration (9.75 %ID/g at 2 min); rapid brain washout (0.72 %ID/g at 60 min); and specific binding to amyloid plaques in AD brain homogenates and sections. However, the increasing bone uptake of radioactivity with time, reaching 7.8 %ID/g at 2 hr postinjection, indicates that the defluorination of [^{18}F]FMAPO is likely to occur *in vivo* [123].

Another series of F-18 labeled stilbene derivatives ([^{18}F]**64**-[^{18}F]**67**) was also developed by Kung and co-workers [124]. Fluorinated polyethylene glycol (PEG) units (n=2-5) were attached to stilbene derivatives on the 4'-hydroxy group of SB-13 to lower

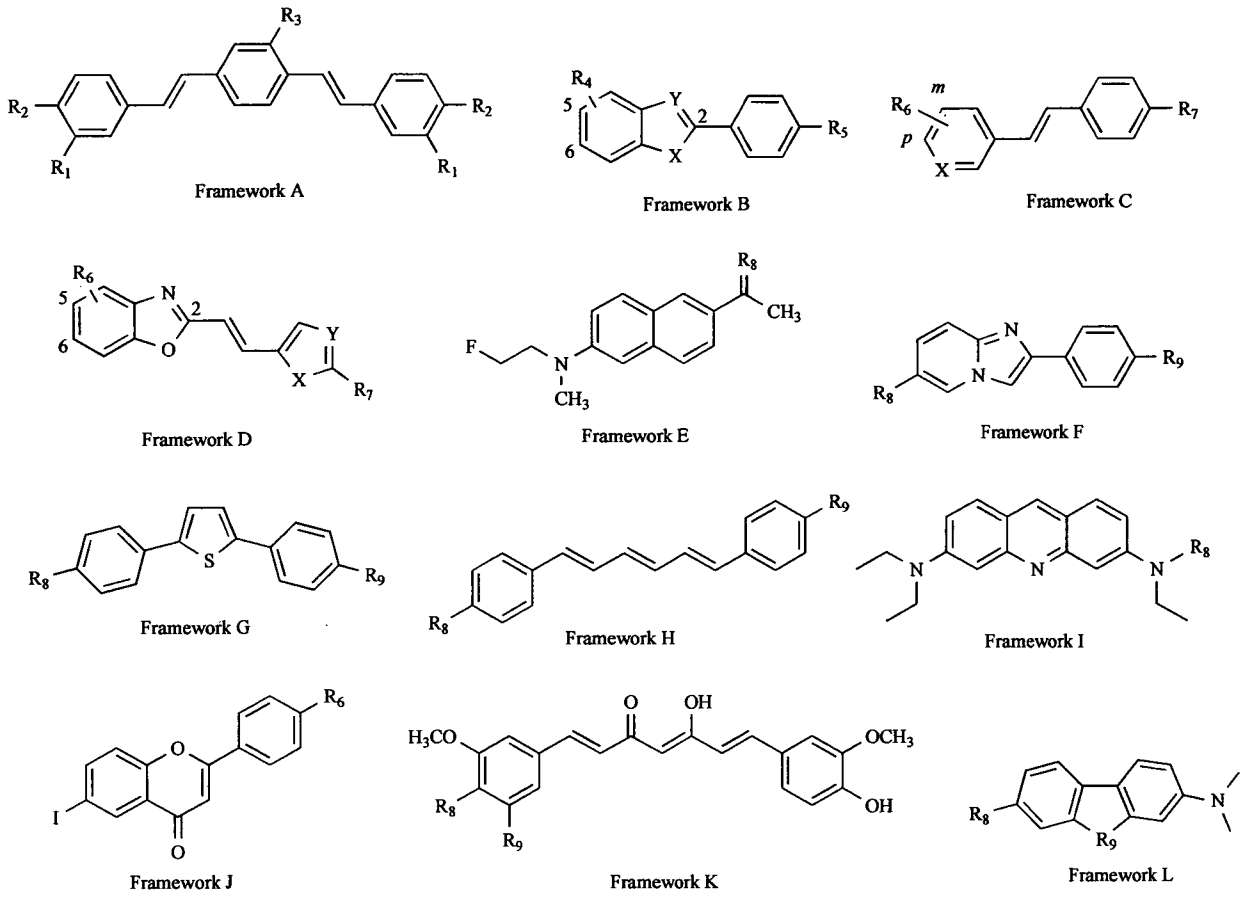

Fig. (4). Molecular frameworks of Aβ ligands that have been reported to date. Each substitution (R_1-R_9) is indicated in Tables **1** ~ **4**.

the lipophilicity and improve bioavailability. The addition of a fluorinated PEG group had little effect on the high binding affinity and the moderate lipophilicity of the parent stilbene derivative. Consequently, these fluorinated PEG stilbene derivatives indicated high binding affinities for amyloid plaques and good pharmacokinetic properties. While defluorination of these derivatives was also detected in the biodistribution studies, the bone uptake values were relatively low (1.5-2.8 %ID/g) in comparison to [^{18}F]FMAPO and related derivatives.

These fluorinated PEG units were introduced to other types of amyloid ligands including PIB, IMPY, BF-168 (**89**) and styrylpyridine derivatives (**80-82**) [125]. These derivatives (**26-29, 77-79, 95-97, 109-113**), containing fluorinated PEG, displayed the same degree of binding affinities as the corresponding parent compounds [126,127]. PIB derivatives (**26-29**) showed moderately favorable brain pharmacokinetics in the case of shorter PEG length (n=2), but high bone uptake was simultaneously observed. IMPY derivatives (**109-113**) exhibited low brain uptake and slow brain clearance. Styrylpyridine derivatives (**77-79**) [127], having the same framework of stilbene, displayed high binding affinities for amyloid plaques and preferable brain kinetics, similar to FMAPO.

5.6. Vinylbezoxazole Derivatives

The vinylbezoxazole derivatives, indicated as Framework D in Fig. (**4**), were recently reported by Kudo and co-workers as promising candidate amyloid imaging agents (**83-94**) [128-131]. These derivatives contain not only a benzoazole and an aromatic ring in their structures, like ThT derivatives, but also a double bond between them, like stilbene derivatives. A competitive binding assay using [^{125}I]**93** (BF-180) and synthetic Aβ aggregates indicated sufficiently high binding affinities for use as Aβ ligands. Although the molecular size of the 2-vinylbenzoxazole derivatives is slightly larger than that of ThT and stilbene derivatives, these three types of derivatives appear to share a common binding site on Aβ aggregates, because the 2-vinylbenzoxazole derivative **89** (BF-168) and the related analogue 2-(4-dimethylaminostyryl)benzothiazole inhibit the binding to Aβ of [^{125}I]IMPY and [^{125}I]TZDM, respectively, at nanomolar concentrations [120,126].

Kudo and co-workers first evaluated a series of 2-styrylbenzoazole derivatives on the basis of their binding affinities for Aβ aggregates, binding selectivity to amyloid plaques (fluorescent staining), and brain uptake *in vivo*, and then selected **89** (BF-168) as a lead compound for amyloid imaging studies. A biodistribution study of [^{18}F]BF-168 in normal mice showed good initial brain uptake and moderately favorable clearance [130]. However, *ex vivo* autoradiography of [^{18}F]BF-168 in normal rat indicated slight residual radioactivity in the white matter [128]. Thus, these authors further synthesized and evaluated several derivatives related to BF-168, and then developed an optimal compound, **94** (BF-227), with regard to brain pharmacokinetics.

Replacement of the phenyl ring of BF-168 with a thiazole ring resulted in no change in the binding affinity of this compound for Aβ aggregates; namely, compound BF-227 exhibited high binding affinities for Aβ40 (Ki: 1.5 nM) and Aβ42 (Ki: 4.9 nM) [132]. A brain uptake study of [^{11}C]BF-227 demonstrated excellent brain penetration (7.9 %ID/g at 2 min) and rapid clearance from the brain (0.72 %ID/g at 60 min). *In vitro* autoradiography of [^{11}C]BF-227

Table 1. Binding affinities (Ki, nM) of the Ligands with Framework A for Aβ Aggregates ($A\beta_{40}$ and/or $A\beta_{42}$) or AD Brain Homogenates (AD-BH) and the Log P_{Oct} Values

Compound No		Framework	R_1	R_2	R_3	Ki (nM)	Log P_{Oct}	Amyloid sample	Ref
1	(X-34)	A	CO_2H	OH	H	18	0.42	$A\beta_{40}$	[27]
2		A	CO_2H	OCH_3	H	47	-0.95	$A\beta_{40}$	[27]
3		A	CO_2H	H	H	135	0.39	$A\beta_{40}$	[27]
4		A	CO_2CH_3	OH	H	119	3.4	$A\beta_{40}$	[27]
5		A	H	OH	OH	9	-	$A\beta_{40}$	[27]
6		A	OH/OCH_3	OH	H	18	-	$A\beta_{40}$	[27]
7	(Me-X34)[a]	A	CO_2H	OH/OCH_3	H	-	-	$A\beta_{40}$	[98]
8	(MeX04)	A	H	OH	OCH_3	26.8[b], 19.5[c]	2.6	$A\beta_{40}$	[98, 27]
9	(BSB)	A	CO_2H	OH	Br	400	-	Aβ	[99]
10	(ISB)	A	CO_2H	OH	I	0.08[d], 0.15[c]	1.54	$A\beta_{40}$, $A\beta_{42}$	[100]
11	(IMSB)	A	CO_2H	OCH_3	I	0.13[d], 0.73[c]	0.04	$A\beta_{40}$, $A\beta_{42}$	[100]
12	(FESB)[a]	A	H	OCH_3	OCH_2CH_2F	-	-	-	[101]

[a] Ki values were not reported in the references. [b] Ki value for $A\beta_{40}$ aggregates. [c] Ki value for $A\beta_{42}$ aggregates.

Table 2. Binding Affinities (Ki, nM) of the Ligands with Framework B for Aβ Aggregates ($A\beta_{40}$ and/or $A\beta_{42}$) or AD Brain Homogenates (AD-BH) and the Log P_{Oct} Values

Compound No		Frame-work	X	Y	R_4	R_5	Ki (nM)	Log P_{Oct}	Amyloid sample	Ref
13	(BTA-0)	B	S	N	H	NH_2	37	2.0[a]	$A\beta_{40}$	[84]
14	(BTA-1)	B	S	N	H	$NHCH_3$	11	2.7[a]	$A\beta_{40}$	[103, 84]
15	(BTA-2)	B	S	N	H	$N(CH_3)_2$	4.0	3.4[a]	$A\beta_{40}$	[84]
16		B	S	N	6-CH_3	$NHCH_3$	10	3.1[a]	$A\beta_{40}$	[103, 84]
17		B	S	N	6-CH_3	$N(CH_3)_2$	64	3.8[a]	$A\beta_{40}$	[103, 84]
18		B	S	N	6-OCH_3	$NHCH_3$	4.9	2.6[a]	$A\beta_{40}$	[84]
19		B	S	N	6-OCH_3	$N(CH_3)_2$	1.9	3.3[a]	$A\beta_{40}$	[84]
20	(PIB)	B	S	N	6-OH	$NHCH_3$	4.3	1.2[a]	$A\beta_{40}$	[84]
21		B	S	N	6-OH	$N(CH_3)_2$	4.4	2.0[a]	$A\beta_{40}$	[84]
22		B	S	N	6-Br	$NHCH_3$	1.7	3.6[a]	$A\beta_{40}$	[84]
23		B	S	N	6-Br	$N(CH_3)_2$	2.9	4.4[a]	$A\beta_{40}$	[84]
24		B	S	N	6-CN	$NHCH_3$	8.6	2.5[a]	$A\beta_{40}$	[84]
25		B	S	N	6-CN	$N(CH_3)_2$	11	3.2[a]	$A\beta_{40}$	[84]
26		B	S	N	6-$(OCH_2CH_2)_2F$	$NHCH_3$	2.2	3.04	AD-BH	[126]
27		B	S	N	6-$(OCH_2CH_2)_3F$	$NHCH_3$	2.8	3.04	AD-BH	[126]
28		B	S	N	6-$(OCH_2CH_2)_6F$	$NHCH_3$	4.7	2.99	AD-BH	[126]
29		B	S	N	6-$(OCH_2CH_2)_8F$	$NHCH_3$	9.0	-	AD-BH	[126]

(Table 2) Contd....

Compound No		Frame -work	X	Y	R_4	R_5	Ki (nM)	Log P_{Oct}	Amyloid sample	Ref
30		B	S	N	6-OCH_3	OH	4.2	1.8	$A\beta_{40}$	[105]
31		B	S	N	6-NO_2	$NHCH_3$	2.75	2.96	$A\beta_{40}$	[105]
32		B	S	N	6-NH_2	OCH_3	6.9	1.76	$A\beta_{40}$	[105]
33		B	S	N	H	F	9	2.76	AD-BH	[115]
34		B	S	N	6-CH_3	F	5.7	-	AD-BH	[116]
35	(TZDM)	B	S	N	6-I	$N(CH_3)_2$	0.06[b], 0.14[c]	1.84	$A\beta_{40}$, $A\beta_{42}$	[100]
36	(TZPI)	B	S	N	6-I	4-methylpiperazin-1-yl	0.13[b], 0.15[c]	2.49	$A\beta_{40}$, $A\beta_{42}$	[100]
37	(IBOX)	B	O	N	6-I	$N(CH_3)_2$	0.8	2.09	$A\beta_{40}$	[107]
38		B	S	C	H	OCH_3	0.40[d], 0.52[e]	3.07	$A\beta_{40}$, $A\beta_{42}$	[117]
39		B	S	C	H	OH	3.04[d], 3.72[e]	2.99	$A\beta_{40}$, $A\beta_{42}$	[117]
40		B	S	C	H	OCH_2CH_2F	0.67[d], 0.87[e]	2.83	$A\beta_{40}$, $A\beta_{42}$	[117]
41		B	S	C	H	$OCH_2CH_2CH_2F$	0.65[d], 0.73[e]	2.88	$A\beta_{40}$, $A\beta_{42}$	[117]
42		B	S	C	H	NH_2	4.31[d], 6.50[e]	2.87	$A\beta_{40}$, $A\beta_{42}$	[117]
43		B	S	C	H	$NHCH_3$	0.28[d], 0.72[e]	3.20	$A\beta_{40}$, $A\beta_{42}$	[117]
44		B	S	C	H	$N(CH_3)_2$	1.06[d], 0.63[e]	3.44	$A\beta_{40}$, $A\beta_{42}$	[117]
45		B	S	C	H	$NHCH_2CH_2F$	1.56[d], 0.98[e]	3.46	$A\beta_{40}$, $A\beta_{42}$	[117]
46		B	S	C	H	$NHCH_2CH_2CH_2F$	0.73[d], 0.77[e]	3.56	$A\beta_{40}$, $A\beta_{42}$	[117]
47		B	O	C	5-OCH_3	NH_2	2.3	-	AD-BH	[108]
48		B	O	C	5-OH	NH_2	11.5	-	AD-BH	[108]
49		B	O	C	5-OCH_3	$NHCH_3$	1.3	-	AD-BH	[108]
50		B	O	C	5-OH	$NHCH_3$	0.7	2.36	AD-BH	[108]
51		B	O	C	5-OCH_3	$N(CH_3)_2$	12.0	-	AD-BH	[108]
52		B	O	C	5-OH	$N(CH_3)_2$	2.8	-	AD-BH	[108]
53		B	O	C	5-Br	$NHCH_3$	2.7	-	$A\beta_{40}$	[109]
54		B	O	C	5-Br	OCH_3	1.3	-	$A\beta_{40}$	[109]

[a] Log P values determined by reverse phase HPLC methods [84]. [b] Kd (nM) for $A\beta_{40}$ aggregates. [c] Kd value (nM) for $A\beta_{42}$ aggregates. [d] Ki value for $A\beta_{40}$ aggregates. [e] Ki value for $A\beta_{42}$ aggregates.

Table 3. Binding Affinities (Ki, nM) of the Ligands with Framework C and D for Aβ Aggregates ($A\beta_{40}$ and/or $A\beta_{42}$) or AD Brain Homogenates (AD-BH), and the Log P_{Oct} Values

Compound No		Frame -work	X	Y	R_6	R_7	Ki (nM)	Log P_{Oct}	Amyloid sample	Ref
55		C	C	-	*m*-I	$N(CH_3)_2$	4.5	-	$A\beta_{40}$	[120]
56		C	C	-	*p*-I	$N(CH_3)_2$	2.0	-	$A\beta_{40}$	[120]
57		C	C	-	*p*-F	$N(CH_3)_2$	22	-	$A\beta_{40}$	[120]
58		C	C	-	*p*-OCH_3	NO_2	151	-	$A\beta_{40}$	[122]

(Table 3) Contd....

Compound No		Frame -work	X	Y	R_6	R_7	Ki (nM)	Log P_{oct}	Amyloid sample	Ref
59		C	C	-	*p*-OCH_3	NH_2	36	-	$A\beta_{40}$	[122]
60		C	C	-	*p*-OCH_3	$NHCH_3$	1.2	-	$A\beta_{40}$	[122]
61	(SB-13)	C	C	-	*p*-OH	$NHCH_3$	6.0	2.36	$A\beta_{40}$	[122]
62		C	C	-	*p*-OCH_3	$N(CH_3)_2$	1.3	-	$A\beta_{40}$	[122]
63		C	C	-	*p*-OH	$N(CH_3)_2$	1.2	-	$A\beta_{40}$	[122]
64		C	C	-	*p*-$(OCH_2CH_2)_2F$	$NHCH_3$	2.9	2.52	AD-BH	[124]
65		C	C	-	*p*-$(OCH_2CH_2)_3F$	$NHCH_3$	6.7	2.41	AD-BH	[124]
66		C	C	-	*p*-$(OCH_2CH_2)_4F$	$NHCH_3$	4.4	2.05	AD-BH	[124]
67		C	C	-	*p*-$(OCH_2CH_2)_5F$	$NHCH_3$	6.0	2.28	AD-BH	[124]
68		C	C	-	*p*-OH	NH_2	95	-	AD-BH	[123]
69		C	C	-	*p*-$OCH_2CH(CH_2OH)CH_2F$	NH_2	15	-	AD-BH	[123]
70		C	C	-	*p*-OH	$N(CH_3)_2$	1.1	-	AD-BH	[123]
71		C	C	-	*p*-$OCH_2CH(CH_2OH)CH_2F$	$N(CH_3)_2$	15	3.13	AD-BH	[123]
72		C	C	-	*p*-$OCH_2CH(CH_2OH)_2$	$N(CH_3)_2$	38	-	AD-BH	[123]
73	(FMAPO)	C	C	-	*p*-$OCH_2CH(CH_2OH)CH_2F$	$NHCH_3$	5.0	2.94	AD-BH	[123]
74		C	C	-	*p*-$OCH_2CH(CH_2OH)_2$	$NHCH_3$	32.5	-	AD-BH	[123]
75		C	N	-	*p*-$(OCH_2CH_2)_3OH$	NH_2	91.2	-	AD-BH	[127]
76		C	N	-	*p*-$(OCH_2CH_2)_3OH$	$N(CH_3)_2$	2.2	-	AD-BH	[127]
77		C	N	-	*p*-$(OCH_2CH_2)_3F$	NH_2	150	-	AD-BH	[127]
78		C	N	-	*p*-$(OCH_2CH_2)_3F$	$NHCH_3$	10	-	AD-BH	[127]
79		C	N	-	*p*-$(OCH_2CH_2)_3F$	$N(CH_3)_2$	2.5	3.22	AD-BH	[127]
80		C	N	-	*p*-Br	$NHCH_3$	7.0	-	AD-BH	[125
81		C	N	-	*p*-Br	$N(CH_3)_2$	3.2	-	AD-BH	[125]
82		C	N	-	*p*-I	$N(CH_3)_2$	4.8	1.92	AD-BH	[125]
83	(BF-133)	D	C=C	C	5-F	$N(CH_3)_2$	2.1[a], 3.4[b]	-	$A\beta_{40}$, $A\beta_{42}$	[129]
84	(BF-145)	D	C=C	C	5-F	$NHCH_3$	3.0[a], 4.5[b]	-	$A\beta_{40}$, $A\beta_{42}$	[129]
85	(BF-140)	D	C=C	C	5-F	NH_2	4.7[a], 2.1[b]	-	$A\beta_{40}$, $A\beta_{42}$	[129]
86	(BF-164)	D	C=C	C	6-H	NH_2	0.38	-	$A\beta_{42}$	[130]
87	(BF-169)	D	C=C	C	6-H	$NHCH_3$	7.1	-	$A\beta_{42}$	[130]
88	(BF-165)	D	C=C	C	6-OH	$NHCH_3$	1.8	-	$A\beta_{42}$	[130]
89	(BF-168)	D	C=C	C	6-OCH_2CH_2F	$NHCH_3$	2.5[a], 6.4[b]	1.79	$A\beta_{40}$, $A\beta_{42}$	[130]
90	(N-282)	D	C=C	C	6-H	$N(CH_3)_2$	4.3	-	$A\beta_{42}$	[130]
91	(BF-148)	D	C=C	C	6-F	$N(CH_3)_2$	4.2	-	$A\beta_{42}$	[130]
92	(BF-125)	D	C=C	C	6-H	$N(CH_2CH_3)_2$	1.5[a], 4.9[b]	-	$A\beta_{40}$, $A\beta_{42}$	[130]
93	(BF-180)	D	C=C	C	5-I	$N(CH_3)_2$	6.7[a], 10.6[b]	-	$A\beta_{40}$, $A\beta_{42}$	[130]
94	(BF-227)	D	S	N	6-OCH_2CH_2F	$N(CH_3)_2$	1.8[a], 4.3[b]	1.75	$A\beta_{40}$, $A\beta_{42}$	[132]

(Table 3) Contd....

Compound No		Frame -work	X	Y	R_6	R_7	Ki (nM)	Log P_{Oct}	Amyloid sample	Ref
95		D	C=C	C	6-$(OCH_2CH_2)_3F$	$N(CH_3)_2$	14.5	2.93	AD-BH	[126]
96		D	C=C	C	6-$(OCH_2CH_2)_6F$	$N(CH_3)_2$	10.0	-	AD-BH	[126]
97		D	C=C	C	6-$(OCH_2CH_2)_8F$	$N(CH_3)_2$	6.0	-	AD-BH	[126]

[a] Ki value for $A\beta_{40}$ aggregates. [b] Ki value for $A\beta_{42}$ aggregates.

Table 4. Binding Affinities (Ki, nM) of the Ligands with Framework E~L for Aβ Aggregates ($A\beta_{40}$ and/or $A\beta_{42}$) or AD Brain Homogenates (AD-BH) and the Log P_{Oct} Values

Compound No		Frame -work	R_8	R_9	Ki (nM)	Log P_{Oct}	Amyloid sample	Ref
98	(FDDNP)	E	$C(CN)_2$	-	0.12(H)[a], 1.86(L)[b]	-	$A\beta_{40}$	[136]
99	(FENE)	E	O	-	0.16(H)[a], 71.2(L)[b]	-	$A\beta_{40}$	[136]
100	(IMPY)	F	I	$N(CH_3)_2$	15	2.18	$A\beta_{40}$	[110]
101		F	CH_3	$N(CH_3)_2$	242	-	$A\beta_{40}$	[111]
102		F	Br	$N(CH_3)_2$	10.3	-	$A\beta_{40}$	[111]
103		F	CH_3	Br	638	-	$A\beta_{40}$	[111]
104		F	$N(CH_3)_2$	Br	339	-	$A\beta_{40}$	[111]
105	(FEM-IMPY)	F	I	$N(CH_3)CH_2CH_2F$	27	4.41	$A\beta_{40}$	[118]
106	(FPM-IMPY)	F	I	$N(CH_3)CH_2CH_2CH_2F$	40	4.60	$A\beta_{40}$	[118]
107	(FEPIP)	F	CH_2CH_2F	$N(CH_3)_2$	177	2.42	$A\beta_{40}$	[119]
108	(FPPIP)	F	$CH_2CH_2CH_2F$	$N(CH_3)_2$	48.3	2.84	$A\beta_{40}$	[119]
109		F	$(OCH_2CH_2)_1F$	$N(CH_3)_2$	16	-	AD-BH	[126]
110		F	$(OCH_2CH_2)_2F$	$N(CH_3)_2$	31	-	AD-BH	[126]
111		F	$(OCH_2CH_2)_3F$	$N(CH_3)_2$	30	2.69	AD-BH	[126]
112		F	$(OCH_2CH_2)_6F$	$N(CH_3)_2$	96	-	AD-BH	[126]
113		F	$(OCH_2CH_2)_8F$	$N(CH_3)_2$	387	-	AD-BH	[126]
114		G	OH	OH	4.0	-	AD-BH	[141]
115		G	OH	OCH_3	6.1	-	AD-BH	[141]
116		G	NH_2	NH_2	6.1	-	AD-BH	[141]
117		G	OCH_3	NO_2	18.5	-	AD-BH	[141]
118		G	OCH_3	NH_2	5.6	-	AD-BH	[141]
119		G	OH	NH_2	9.6	-	AD-BH	[141]
120		G	OH	$N(CH_3)_2$	7.5	-	AD-BH	[141]
121		G	OCH_3	$NHCH_2CH_2F$	21.5	-	AD-BH	[141]
122		G	OH	$NHCH_2CH_2F$	3.9	-	AD-BH	[141]
123		G	OH	$NHCH_3$	31.2	-	AD-BH	[141]
124		H	OH	OH	9.0[c], 150[d]	-	AD-BH	[142]

(Table 4) Contd....

Compound No		Frame -work	R_8	R_9	Ki (nM)	Log P_{oct}	Amyloid sample	Ref
125		H	NH_2	NH_2	9.0[e], 375[d]	-	AD-BH	[142]
126		H	$NHCH_3$	$NHCH_3$	7.5[e], 122[d]	-	AD-BH	[142]
127		H	NH_2	$NHCH_2CH_2F$	12[e], 217[d]	-	AD-BH	[142]
128	(BF-108)	I	CH_2CH_2F	-	135[e]	3.01	$A\beta_{40}$	[144]
129		J	$NHCH_3$	-	22.6[e], 30.0[d]	2.15	$A\beta_{40}$, $A\beta_{42}$	[149]
130		J	$N(CH_3)_2$	-	13.2[e], 15.6[d]	2.69	$A\beta_{40}$, $A\beta_{42}$	[149]
131		J	OCH_3	-	29.0[e], 38.3[d]	2.41	$A\beta_{40}$, $A\beta_{42}$	[149]
132		J	OH	-	72.5[e], 77.2[d]	1.92	$A\beta_{40}$, $A\beta_{42}$	[149]
133		K	OH	I	9.37	0.94	$A\beta_{40}$	[151]
134		K	$OCH_2CH_2CH_2F$	H	0.07	1.84	$A\beta_{40}$	[151]
135		L	Br	CO	16.5	-	$A\beta_{40}$	[140]
136		L	Br	CH_2	0.85	-	$A\beta_{40}$	[140]
137		L	I	CH_2	0.92	2.46	$A\beta_{40}$	[140]

[a] Kd value (nM) for high-affinity binding site of $A\beta_{40}$ aggregates. [b] Kd value (nM) for low-affinity binding site of $A\beta_{40}$ aggregates. [c] Ki value for $A\beta_{40}$ aggregates. [d] Ki value for $A\beta_{42}$ aggregates. [e] IC_{50} value for $A\beta_{40}$ aggregates determined by fluorometric ThT method.

clearly indicated specific binding to amyloid plaques in AD brain tissue sections [133]. These results suggest that [^{11}C]BF-227 is a promising radioligand for the imaging of Aβ plaques.

5.7. DDNP Derivatives

The compound 2-(1-(6-(dimethylamino)naphthalen-2-yl)ethylidene)malononitrile (DDNP) is a neutral and lipophilic fluorescent probe that is sensitive to solvent polarity and viscosity [134]. Barrio and co-workers applied a fluorinated derivative of DDNP (**98**, FDDNP, see Framework E in Fig. (**4**)) as a PET radioligand for imaging AD brain pathology [135-137]. Fluorescent staining of AD brain sections revealed that FDDNP intensely labels the dense core and diffuse plaques, and faintly labels NFTs. Fluorescence titration assays of FDDNP indicated a high binding affinity for Aβ aggregates (Kd: 0.12 (high), 1.86 (low) nM) [136]. Competition assays with [^{18}F]FDDNP against CR and ThT indicated that the binding site for FDDNP on Aβ aggregates is different from those of CR and ThT [138]. High binding affinity was also ascertained by a radiobinding assay using [^{18}F]FDDNP and AD brain homogenates (Kd: 0.75 nM) [137]. Data on the brain uptake of [^{18}F]FDDNP in small animals (mouse, rat) have not yet been reported.

5.8. Miscellaneous Derivatives

Currently, a variety of molecular frameworks have been applied to the development of amyloid imaging agents. In addition to the above-mentioned amyloid ligands, Kung and co-workers have reported other types of amyloid ligands, including derivatives of fluorene, biphenyl thiophene, and biphenyltriene, represented as Frameworks L, G, and H, respectively, in Fig. (**4**). A preliminary study of the structure-activity relationship of fluorene derivatives (**135-137**) demonstrated that some derivatives had a high binding affinity for Aβ aggregates [139,140]. However, a biodistribution study using [^{125}I]**137** indicated moderate brain uptake and slow brain clearance.

Based on the successful development of stilbene derivatives for amyloid imaging, Kung and co-workers have focused on the highly conjugated biphenyl derivatives as candidate amyloid imaging agents. To build a highly conjugated structure between two phenyl rings, they replaced the double bond in stilbene-based probes with thiophene, which can be considered as a diene in an *s-cis* conformation. These derivatives carrying at least one hydroxy or primary/secondary amino group in the phenyl ring (**114-123**) showed effective binding affinities for AD brain homogenates [141]. Further study to develop PET amyloid imaging agents based on these derivatives is currently under way. Another group of highly conjugated derivatives, biphenyltrienes (**124-127**), exhibited not only high affinities for the IMPY binding site on the Aβ aggregates, but also moderate affinities for the IMSB binding site [142].

Kudo and co-workers have reported that acridine orange and its derivative (**128**, BF-108) show potent binding to Aβ aggregates, and fluorescently label NPs and NFTs in AD brain sections [143,144]. However, a biodistribution study of [^{18}F]BF-108 displayed unfavorably slow and low brain uptake in normal mice.

As a new approach to the development of amyloid imaging agents, natural product-based radioligands have been explored. Flavones and curcumin have been demonstrated to inhibit the formation and extension of Aβ fibrils, and to destabilize preformed Aβ fibrils [145-147]. These results imply that flavones and curcumin could have potential for binding to Aβ fibrils. Indeed, curcumin was recently shown to fluorescently label Aβ plaques in AD brain sections [148], indicating its binding potency to Aβ fibrils.

Ono and co-workers clarified that iodinated flavone derivatives ([^{125}I]**129**-[^{125}I]**132**) possess high binding affinities for Aβ aggregates; stain NPs and NFTs in AD brain sections; and show good brain uptake and clearance in mice [149]. A notable finding in their study is that the flavone derivatives may have a unique binding site on Aβ aggregates that is different from those of ThT and CR. Since these binding profiles, including NFT staining, of the flavone derivatives are fairly similar to those of FDDNP, it is of particular interest whether their binding sites on Aβ aggregates are

identical to each other or not. Ono and co-workers recently reported a series of 2-styrylchromone derivatives, flavone-related derivatives, in which the 2-phenyl substituent of the flavone backbone is replaced with the 2-styryl substituent [150].

Ryu and co-workers synthesized and evaluated an F-18-labeled curcumin derivative ([^{18}F]**134**) [151]. Compound **134** exhibited excellent binding affinity for the IMSB (CR) binding site (Ki: 0.07 nM). However, a biodistribution study elucidated that the brain entry of [^{18}F]**134** was inadequate (0.52 %ID/g at 2 min), probably due to rapid metabolism in the liver (39 %ID/g at 2 min) and in the intestinal wall, like curcumin. In an attempt to improve brain uptake, co-administration of [^{18}F]**134** with piperine, which is known to increase the bioavailability of curcumin, was also examined; however, the effect was limited.

6. HUMAN PET STUDIES OF AMYLOID IMAGING AGENTS

Among the amyloid imaging agents described above, [^{11}C]PIB, [^{11}C]SB-13, [^{11}C]BF-227, and [^{18}F]FDDNP have been evaluated in preliminary clinical studies. Of these tracers, [^{11}C]PIB is the most widely evaluated in clinical PET studies all over the world. Despite the small number of subjects, these studies have demonstrated sufficiently promising results in amyloid imaging studies.

The initial human PET study of [^{11}C]PIB was conducted in 9 healthy control subjects and 15 AD patients to provide a "proof of concept" for imaging amyloid plaques in the brains of AD patients [152]. In the healthy control group, time-activity data, expressed as semiquantitative standardized uptake values (SUVs) of [^{11}C]PIB, indicated rapid brain entrance and clearance of [^{11}C]PIB in all cortical areas including the cerebellar cortex. The time-activity curves of [^{11}C]PIB in AD patients exhibited relatively slower clearances in the cortical regions found to contain significant levels of Aβ plaques on postmortem examination, such as the parietal and frontal cortices. In the cerebellum, an area lacking fibrillar amyloid plaques, nearly identical time-activity curves were obtained in healthy control subjects and AD patients. PIB-SUV images summed over 40 to 60 min showed clear differences in the topographical distribution pattern of [^{11}C]PIB accumulation between healthy control subjects and AD patients. In accordance with the distribution pattern of Aβ deposition [153,154], [^{11}C]PIB was markedly retained in the corresponding cortical areas of AD patients, but there was little or no retention in these areas of healthy control subjects, while white matter areas indicated some retention to the same degree in both healthy control subjects and AD patients, presumably due to non-specific binding. The [^{11}C]PIB retentions (SUVs) in the cortical areas of AD patients, including frontal, parietal, temporal, and occipital cortices, were 1.5~1.9-fold higher than those of healthy control subjects. These studies indicate that [^{11}C]PIB has enough potential to visualize the degree and distribution of Aβ deposits in the cortical regions of AD brain.

To use amyloid imaging for AD diagnosis and to assess anti-amyloid therapy, it is necessary to establish a valid and reliable quantitative method for the measurement of Aβ deposition. With regard to the analysis of PIB-PET data, several quantitative methods were evaluated in detail, and the Logan analysis was proven to be the method-of-choice for stable and valid analytical results [155]. In addition, non-invasive Logan analysis and SUV ratio analysis, simplified methods that used cerebellum as a reference region, were confirmed to be effective as well as quantitative arterial-based analysis [156]. These methods would contribute to studies with large subject populations (e.g. clinical trials) or that are difficult to carry out (e.g. severe AD subjects, the sampling of whose arterial blood is difficult). PIB analysis according to a voxel-based method has also been reported to be robust for the assessment of differences in [^{11}C]PIB retention between control subjects and mild-to-moderate AD patients [157].

Recently, several research groups have reported the clinical application of PIB-PET for the study of AD [158-161]. PIB imaging in MCI subjects revealed that the degree of [^{11}C]PIB retention is bimodally distributed, with higher levels in AD patients (PIB positive) and lower levels in healthy controls (PIB negative) [156]; the proportion of PIB-positive subjects with MCI was 50% to 60% [30]. Furthermore, elevated [^{11}C]PIB retentions were observed even in cognitively normal subjects [162,163]. These results suggest that PIB amyloid imaging might be sufficiently sensitive for the earlier identification of AD patients who have amyloid plaques in their brains, in the early stages of MCI or even in the presymptomatic disease state.

A human PET study of [^{11}C]SB-13 was performed to evaluate its potential as an amyloid imaging agent by comparing it with [^{11}C]PIB in AD patients and healthy control subjects [164]. In AD patients, both radiotracers showed significantly higher retention in cortical regions compared to healthy control subjects, and the relative cortical uptakes were higher for [^{11}C]SB-13 than for [^{11}C]PIB. In a comparative evaluation between AD and control subjects, the binding potentials derived from SB-13 imaging were highly discriminated in the frontal and occipital cortices, while the potentials from PIB imaging showed higher discriminations not only in those cortices, but also in the temporal cortex. Although slight differences were found, [^{11}C]SB-13 seems to be an effective PET tracer for imaging Aβ deposits in AD brain, with similar performance to [^{11}C]PIB.

Fairly recently, amyloid imaging with [^{11}C]BF-227 has been evaluated in AD patients and healthy control subjects [132]. In control subjects, [^{11}C]BF-227 showed rapid brain uptake and clearance in cortical regions. However, AD patients showed slower-than-normal clearances of [^{11}C]BF-227 in the frontal, temporal, and parietal cortices, while brain uptake was rapid in AD patients as well as in control subjects. In contrast to the cortical regions, the brain uptake and clearance in the cerebellum was nearly identical between control subjects and AD patients. Compared to control subjects, the SUV images summed over 20 to 40 min post injection clearly demonstrated the cortical retention of [^{11}C]BF-227, especially in the basal portion of the frontal, temporal and parietal regions, in AD patients. The voxel-by-voxel analysis of [^{11}C]BF-227 showed significantly higher cortical retentions in the temporo-parietal-occipital regions rather than the frontal region and striatum, in AD patients compared with controls; these regions correspond to the regions containing a high density of NPs, as indicated by postmortem pathological studies [153]. All AD patients were clearly distinguishable from control subjects using the SUV ratio in the temporal cortex. These results suggest that [^{11}C]BF-227 is a potent PET probe for the *in vivo* detection of amyloid deposits in AD patients.

[^{18}F]FDDNP was the first PET probe reported to be effective in the visualization of neuropathology in the living brains of AD patients [165,166]. Administered [^{18}F]FDDNP showed good brain penetration and specific retention in the hippocampus, amygdala and entorhinal regions in AD patients. As expected from the *in vitro* binding property of FDDNP, these brain regions matched the distribution area of dense NPs and NFT depositions, as determined by postmortem neuropathological studies of AD patients. The greater degree of [^{18}F]FDDNP accumulation in these brain regions correlated well with lower memory performance scores. Recent research demonstrated that FDDNP-PET scanning can discriminate between persons with MCI, those with AD and those with no cognitive impairment [167]. Although FDDNP-PET is not suited to the specific evaluation of Aβ deposition in the AD brain, it could be useful for assessing the neuropathological progression of the disease.

7. CONCLUDING REMARKS

During the last few years, remarkable progress has been made in the development of radioligands or other candidates for *in vivo* imaging of Aβ deposits in the AD brain. The concept of amyloid imaging is currently being tested in human PET studies with some of these radioligands, and its potential for clinical application is now becoming apparent. To verify the validity of amyloid imaging completely, it is necessary that a follow-up of subjects with or without AD be performed after PET scanning for amyloid imaging, including postmortem evaluation to confirm whether the extent and distribution of Aβ loads estimated by the amyloid imaging are in accordance with the Aβ pathology in the brains of the same human subjects. Further clinical evaluations of the utility of amyloid imaging, in larger series of AD patients, are also required to determine the usefulness of amyloid imaging in the early diagnosis of AD, or in the assessment of the clinical efficacy of anti-amyloid therapy. Additionally, in terms of the widespread availability and use of amyloid imaging with PET, there is an urgent need to promote the development of F-18-labeled agents suited to clinical use.

Although a number of issues remain to be addressed, recent promising results from human PET studies encourage the development and refinement of amyloid imaging agents. We really hope that, in the near future, *in vivo* PET imaging for assessing Aβ deposits in the AD brain will greatly contribute to dramatic progress in neuropathological studies of AD in living humans, the early diagnosis of AD, and disease-modifying therapies based on anti-amyloid agents.

ACKNOWLEDGMENTS

This work was supported in part by Special Coordination Funds for Promoting Science and Technology from the Japan Science and Technology Agency; the Health and Labor Sciences Research Grants for Translational Research from the Ministry of Health, Labor and Welfare; and Grants from the Ministry of Education, Science, Sports and Culture, Japan.

REFERENCES

[1] Blennow, K.; de Leon, M. J.; Zetterberg, H. Alzheimer's disease. *Lancet* **2006,** *368*, 387-403.

[2] Cummings, J. L.; Cole, G. Alzheimer disease. *JAMA* **2002,** *287*, 2335-2338.

[3] Drachman, D. A. Aging of the brain, entropy, and Alzheimer disease. *Neurology* **2006,** *67*, 1340-1352.

[4] Hodges, J. R. Alzheimer's centennial legacy: origins, landmarks and the current status of knowledge concerning cognitive aspects. *Brain* **2006,** *129*, 2811-2822.

[5] Morris, J. C.; Kimberly, A.; Quaid, K.; Holtzman, D. M.; Kantarci, K.; Kaye, J.; Reiman, E. M.; Klunk, W. E.; Siemers, E. R. Role of biomarkers in studies of presymptomatic Alzheimer's disease. *Alzheimer Dementia* **2005,** *1*, 145-151.

[6] von Strauss, E.; Viitanen, M.; De Ronchi, D.; Winblad, B.; Fratiglioni, L. Aging and the occurrence of dementia: findings from a population-based cohort with a large sample of nonagenarians. *Arch. Neurol.* **1999,** *56*, 587-592.

[7] Rice, D. P.; Fillit, H. M.; Max, W.; Knopman, D. S.; Lloyd, J. R.; Duttagupta, S. Prevalence, costs, and treatment of Alzheimer's disease and related dementia: a managed care perspective. *Am. J. Manag. Care* **2001,** *7*, 809-818.

[8] Wynn, Z. J.; Cummings, J. L. Cholinesterase inhibitor therapies and neuropsychiatric manifestations of Alzheimer's disease. *Dement. Geriatr. Cogn. Disord.* **2004,** *17*, 100-108.

[9] Schott, J. M.; Kennedy, J.; Fox, N. C. New developments in mild cognitive impairment and Alzheimer's disease. *Curr. Opin. Neurol.* **2006,** *19*, 552-558.

[10] Clark, C. M.; Karlawish, J. H. Alzheimer disease: current concepts and emerging diagnostic and therapeutic strategies. *Ann. Intern. Med.* **2003,** *138*, 400-410.

[11] Parihar, M. S.; Hemnani, T. Alzheimer's disease pathogenesis and therapeutic interventions. *J. Clin. Neurosci.* **2004,** *11*, 456-467.

[12] Hardy, J. A.; Higgins, G. A. Alzheimer's disease: the amyloid cascade hypothesis. *Science* **1992,** *256*, 184-185.

[13] Hardy, J.; Selkoe, D. J. The amyloid hypothesis of Alzheimer's disease: progress and problems on the road to therapeutics. *Science* **2002,** *297*, 353-356.

[14] Verdile, G.; Fuller, S.; Atwood, C. S.; Laws, S. M.; Gandy, S. E.; Martins, R. N. The role of beta amyloid in Alzheimer's disease: still a cause of everything or the only one who got caught? *Pharmacol. Res.* **2004,** *50*, 397-409.

[15] Jacobsen, J. S.; Reinhart, P.; Pangalos, M. N. Current concepts in therapeutic strategies targeting cognitive decline and disease modification in Alzheimer's disease. *NeuroRx* **2005,** *2*, 612-626.

[16] Mason, J. M.; Kokkoni, N.; Stott, K.; Doig, A. J. Design strategies for anti-amyloid agents. *Curr. Opin. Struct. Biol.* **2003,** *13*, 526-532.

[17] Golde, T. E. Alzheimer disease therapy: can the amyloid cascade be halted? *J. Clin. Invest.* **2003,** *111*, 11-18.

[18] Mortimer, J. A.; Borenstein, A. R.; Gosche, K. M.; Snowdon, D. A. Very early detection of Alzheimer neuropathology and the role of brain reserve in modifying its clinical expression. *J. Geriatr. Psychiatry Neurol.* **2005,** *18*, 218-223.

[19] Small, G. W. Diagnostic issues in dementia: neuroimaging as a surrogate marker of disease. *J. Geriatr. Psychiatry Neurol.* **2006,** *19*, 180-185.

[20] Mehta, P. D.; Pirttila, T. Biological markers of Alzheimer's disease. *Drug. Dev. Res.* **2002,** *56*, 74-84.

[21] Nordberg, A. PET imaging of amyloid in Alzheimer's disease. *Lancet Neurol.* **2004,** *3*, 519-527.

[22] Zamrini, E.; De Santi, S.; Tolar, M. Imaging is superior to cognitive testing for early diagnosis of Alzheimer's disease. *Neurobiol. Aging* **2004,** *25*, 685-691.

[23] Sair, H. I.; Doraiswamy, P. M.; Petrella, J. R. *In vivo* amyloid imaging in Alzheimer's disease. *Neuroradiology* **2004,** *46*, 93-104.

[24] Villemagne, V. L.; Rowe, C. C.; Macfarlane, S.; Novakovic, K. E.; Masters, C. L. Imaginem oblivionis: the prospects of neuroimaging for early detection of Alzheimer's disease. *J. Clin. Neurosci.* **2005,** *12*, 221-230.

[25] Huddleston, D. E.; Small, S. A. Technology Insight: imaging amyloid plaques in the living brain with positron emission tomography and MRI. *Nat. Clin. Pract. Neurol.* **2005,** *1*, 96-105.

[26] Kudo, Y. Development of amyloid imaging PET probes for an early diagnosis of Alzheimer's disease. *Minim. Invasive. Ther. Allied. Technol.* **2006,** *15*, 209-213.

[27] Mathis, C. A.; Wang, Y.; Klunk, W. E. Imaging beta-amyloid plaques and neurofibrillary tangles in the aging human brain. *Curr. Pharm. Des.* **2004,** *10*, 1469-1492.

[28] Wu, C.; Pike, V. W.; Wang, Y. Amyloid imaging: from benchtop to bedside. *Curr. Top. Dev. Biol.* **2005,** *70*, 171-213.

[29] Lockhart, A. Imaging Alzheimer's disease pathology: one target, many ligands. *Drug Discov. Today* **2006,** *11*, 1093-1099.

[30] Johnson, K. A. Amyloid imaging of Alzheimer's disease using Pittsburgh Compound B. *Curr. Neurol. Neurosci. Rep.* **2006,** *6*, 496-503.

[31] Masters, C. L.; Cappai, R.; Barnham, K. J.; Villemagne, V. L. Molecular mechanisms for Alzheimer's disease: implications for neuroimaging and therapeutics. *J. Neurochem.* **2006,** *97*, 1700-1725.

[32] Braak, H.; Braak, E. Neuropathological stageing of Alzheimer-related changes. *Acta Neuropathol. (Berl).* **1991,** *82*, 239-259.

[33] Wong, C. W.; Quaranta, V.; Glenner, G. G. Neuritic plaques and cerebrovascular amyloid in Alzheimer disease are antigenically related. *Proc. Natl. Acad. Sci. U. S. A.* **1985,** *82*, 8729-8732.

[34] Delacourte, A.; David, J. P.; Sergeant, N.; Buee, L.; Wattez, A.; Vermersch, P.; Ghozali, F.; Fallet-Bianco, C.; Pasquier, F.; Lebert, F.; Petit, H.; Di Menza, C. The biochemical pathway of neurofibrillary degeneration in aging and Alzheimer's disease. *Neurology* **1999,** *52*, 1158-1165.

[35] Spillantini, M. G.; Goedert, M. Tau protein pathology in neurodegenerative diseases. *Trends Neurosci.* **1998,** *21*, 428-433.

[36] Goedert, M.; Crowther, R. A.; Spillantini, M. G. Tau mutations cause frontotemporal dementias. *Neuron* **1998,** *21*, 955-958.

[37] Kang, J.; Lemaire, H. G.; Unterbeck, A.; Salbaum, J. M.; Masters, C. L.; Grzeschik, K. H.; Multhaup, G.; Beyreuther, K.; Muller-Hill, B. The precursor of Alzheimer's disease amyloid A4 protein resembles a cell-surface receptor. *Nature* **1987,** *325*, 733-736.

[38] Nunan, J.; Small, D. H. Regulation of APP cleavage by alpha-, beta- and gamma-secretases. *FEBS Lett.* **2000,** *483*, 6-10.

[39] Haass, C. Take five--BACE and the gamma-secretase quartet conduct Alzheimer's amyloid beta-peptide generation. *EMBO J.* **2004,** *23*, 483-488.

[40] Wolfe, M. S. The gamma-secretase complex: membrane-embedded proteolytic ensemble. *Biochemistry* **2006,** *45*, 7931-7939.

[41] Johnston, J. A.; Liu, W. W.; Todd, S. A.; Coulson, D. T.; Murphy, S.; Irvine, G. B.; Passmore, A. P. Expression and activity of beta-site amyloid precursor protein cleaving enzyme in Alzheimer's disease. *Biochem. Soc. Trans.* **2005,** *33*, 1096-1100.

[42] Reinhard, C.; Hebert, S. S.; De Strooper, B. The amyloid-beta precursor protein: integrating structure with biological function. *EMBO J.* **2005,** *24*, 3996-4006.

[43] Jarrett, J. T.; Berger, E. P.; Lansbury, P. T., Jr. The carboxy terminus of the beta amyloid protein is critical for the seeding of amyloid formation: implications for the pathogenesis of Alzheimer's disease. *Biochemistry* **1993,** *32*, 4693-4697.

[44] Zlokovic, B. V. Clearing amyloid through the blood-brain barrier. *J. Neurochem.* **2004,** *89*, 807-811.

[45] Saido, T. C.; Iwata, N. Metabolism of amyloid beta peptide and pathogenesis of Alzheimer's disease. Towards presymptomatic diagnosis, prevention and therapy. *Neurosci. Res.* **2006,** *54*, 235-253.

[46] Mann, D. M.; Iwatsubo, T.; Ihara, Y.; Cairns, N. J.; Lantos, P. L.; Bogdanovic, N.; Lannfelt, L.; Winblad, B.; Maat-Schieman, M. L.; Rossor, M. N. Predominant deposition of amyloid-beta 42(43) in plaques in cases of Alzheimer's disease and hereditary cerebral hemorrhage associated with mutations in the amyloid precursor protein gene. *Am. J. Pathol.* **1996,** *148*, 1257-1266.

[47] Hsia, A. Y.; Masliah, E.; McConlogue, L.; Yu, G. Q.; Tatsuno, G.; Hu, K.; Kholodenko, D.; Malenka, R. C.; Nicoll, R. A.; Mucke, L. Plaque-independent disruption of neural circuits in Alzheimer's disease mouse models. *Proc. Natl. Acad. Sci. U. S. A.* **1999,** *96*, 3228-3233.

[48] Westerman, M. A.; Cooper-Blacketer, D.; Mariash, A.; Kotilinek, L.; Kawarabayashi, T.; Younkin, L. H.; Carlson, G. A.; Younkin, S. G.; Ashe, K. H. The relationship between Abeta and memory in the Tg2576 mouse model of Alzheimer's disease. *J. Neurosci.* **2002,** *22*, 1858-1867.

[49] Mucke, L.; Masliah, E.; Yu, G. Q.; Mallory, M.; Rockenstein, E. M.; Tatsuno, G.; Hu, K.; Kholodenko, D.; Johnson-Wood, K.; McConlogue, L. High-level neuronal expression of abeta 1-42 in wild-type human amyloid protein precursor transgenic mice: synaptotoxicity without plaque formation. *J. Neurosci.* **2000,** *20*, 4050-4058.

[50] Pratico, D.; Delanty, N. Oxidative injury in diseases of the central nervous system: focus on Alzheimer's disease. *Am. J. Med.* **2000,** *109*, 577-585.

[51] Sastre, M.; Klockgether, T.; Heneka, M. T. Contribution of inflammatory processes to Alzheimer's disease: molecular mechanisms. *Int. J. Dev. Neurosci.* **2006,** *24*, 167-176.

[52] Hardy, J. Amyloid double trouble. *Nat. Genet.* **2006,** *38*, 11-12.

[53] St George-Hyslop, P. H. Molecular genetics of Alzheimer's disease. *Biol. Psychiatry* **2000,** *47*, 183-199.

[54] Teller, J. K.; Russo, C.; DeBusk, L. M.; Angelini, G.; Zaccheo, D.; Dagna-Bricarelli, F.; Scartezzini, P.; Bertolini, S.; Mann, D. M.; Tabaton, M.; Gambetti, P. Presence of soluble amyloid beta-peptide precedes amyloid plaque formation in Down's syndrome. *Nat. Med.* **1996,** *2*, 93-95.

[55] LaFerla, F. M.; Oddo, S. Alzheimer's disease: Abeta, tau and synaptic dysfunction. *Trends Mol. Med.* **2005,** *11*, 170-176.

[56] McGowan, E.; Eriksen, J.; Hutton, M. A decade of modeling Alzheimer's disease in transgenic mice. *Trends Genet.* **2006,** *22*, 281-289.

[57] Oddo, S.; Caccamo, A.; Shepherd, J. D.; Murphy, M. P.; Golde, T. E.; Kayed, R.; Metherate, R.; Mattson, M. P.; Akbari, Y.; LaFerla, F. M. Triple-transgenic model of Alzheimer's disease with plaques and tangles: intracellular Abeta and synaptic dysfunction. *Neuron* **2003,** *39*, 409-421.

[58] Oddo, S.; Caccamo, A.; Kitazawa, M.; Tseng, B. P.; LaFerla, F. M. Amyloid deposition precedes tangle formation in a triple transgenic model of Alzheimer's disease. *Neurobiol. Aging* **2003,** *24*, 1063-1070.

[59] Sambamurti, K.; Hardy, J.; Refolo, L. M.; Lahiri, D. K. Targeting APP metabolism for the treatment of Alzheimer's disease. *Drug Dev. Res.* **2002,** *56*, 211-227.

[60] Citron, M. Beta-secretase inhibition for the treatment of Alzheimer's disease--promise and challenge. *Trends Pharmacol. Sci.* **2004,** *25*, 92-97.

[61] Walter, J.; Haass, C. Secretases as targets for beta-amyloid lowering drugs. *Drug Dev. Res.* **2002,** *56*, 201-210.

[62] Siemers, E. R.; Quinn, J. F.; Kaye, J.; Farlow, M. R.; Porsteinsson, A.; Tariot, P.; Zoulnouni, P.; Galvin, J. E.; Holtzman, D. M.; Knopman, D. S.; Satterwhite, J.; Gonzales, C.; Dean, R. A.; May, P. C. Effects of a gamma-secretase inhibitor in a randomized study of patients with Alzheimer disease. *Neurology* **2006,** *66*, 602-604.

[63] Eriksen, J. L.; Sagi, S. A.; Smith, T. E.; Weggen, S.; Das, P.; McLendon, D. C.; Ozols, V. V.; Jessing, K. W.; Zavitz, K. H.; Koo, E. H.; Golde, T. E. NSAIDs and enantiomers of flurbiprofen target gamma-secretase and lower Abeta 42 *in vivo*. *J. Clin. Invest.* **2003,** *112*, 440-449.

[64] Gervais, F.; Paquette, J.; Morissette, C.; Krzywkowski, P.; Yu, M.; Azzi, M.; Lacombe, D.; Kong, X.; Aman, A.; Laurin, J.; Szarek, W. A.; Tremblay, P. Targeting soluble Abeta peptide with Tramiprosate for the treatment of brain amyloidosis. *Neurobiol. Aging* **2007,** *28*, 537-547.

[65] Masters, C. L.; Beyreuther, K. Alzheimer's centennial legacy: prospects for rational therapeutic intervention targeting the Abeta amyloid pathway. *Brain* **2006,** *129*, 2823-2839.

[66] Winblad, B.; Wimo, A.; Engedal, K.; Soininen, H.; Verhey, F.; Waldemar, G.; Wetterholm, A. L.; Haglund, A.; Zhang, R.; Schindler, R. 3-year study of donepezil therapy in Alzheimer's disease: effects of early and continuous therapy. *Dement. Geriatr. Cogn. Disord.* **2006,** *21*, 353-363.

[67] Wimo, A.; Winblad, B.; Engedal, K.; Soininen, H.; Verhey, F.; Waldemar, G.; Wetterholm, A. L.; Mastey, V.; Haglund, A.; Zhang, R.; Miceli, R.; Chin, W.; Subbiah, P. An economic evaluation of donepezil in mild to moderate Alzheimer's disease: results of a 1-year, double-blind, randomized trial. *Dement. Geriatr. Cogn. Disord.* **2003,** *15*, 44-54.

[68] Borroni, B.; Di Luca, M.; Padovani, A. Predicting Alzheimer dementia in mild cognitive impairment patients. Are biomarkers useful? *Eur. J. Pharmacol.* **2006,** *545*, 73-80.

[69] Mirra, S. S.; Heyman, A.; McKeel, D.; Sumi, S. M.; Crain, B. J.; Brownlee, L. M.; Vogel, F. S.; Hughes, J. P.; van Belle, G.; Berg, L. The Consortium to Establish a Registry for Alzheimer's Disease (CERAD). Part II. Standardization of the neuropathologic assessment of Alzheimer's disease. *Neurology* **1991,** *41*, 479-486.

[70] Markesbery, W. R. Neuropathological criteria for the diagnosis of Alzheimer's disease. *Neurobiol. Aging* **1997,** *18*, S13-19.

[71] Pupi, A.; Mosconi, L.; Nobili, F. M.; Sorbi, S. Toward the validation of functional neuroimaging as a potential biomarker for Alzheimer's disease: implications for drug development. *Mol. Imaging Biol.* **2005,** *7*, 59-68.

[72] Petersen, R. C.; Smith, G. E.; Waring, S. C.; Ivnik, R. J.; Tangalos, E. G.; Kokmen, E. Mild cognitive impairment: clinical characterization and outcome. *Arch. Neurol.* **1999,** *56*, 303-308.

[73] Tiraboschi, P.; Hansen, L. A.; Thal, L. J.; Corey-Bloom, J. The importance of neuritic plaques and tangles to the development and evolution of AD. *Neurology* **2004,** *62*, 1984-1989.

[74] Price, J. L.; Morris, J. C. Tangles and plaques in nondemented aging and "preclinical" Alzheimer's disease. *Ann. Neurol.* **1999,** *45*, 358-368.

[75] Morris, J. C.; Storandt, M.; Miller, J. P.; McKeel, D. W.; Price, J. L.; Rubin, E. H.; Berg, L. Mild cognitive impairment represents early-stage Alzheimer disease. *Arch. Neurol.* **2001,** *58*, 397-405.

[76] Dickerson, B. C.; Sperling, R. A. Neuroimaging biomarkers for clinical trials of disease-modifying therapies in Alzheimer's disease. *NeuroRx* **2005,** *2*, 348-360.

[77] Thal, L. J.; Kantarci, K.; Reiman, E. M.; Klunk, W. E.; Weiner, M. W.; Zetterberg, H.; Galasko, D.; Pratico, D.; Griffin, S.; Schenk, D.; Siemers, E. The role of biomarkers in clinical trials for Alzheimer disease. *Alzheimer Dis. Assoc. Disord.* **2006,** *20*, 6-15.

[78] Poduslo, J. F.; Wengenack, T. M.; Curran, G. L.; Wisniewski, T.; Sigurdsson, E. M.; Macura, S. I.; Borowski, B. J.; Jack, C. R., Jr. Molecular targeting of Alzheimer's amyloid plaques for contrast-enhanced magnetic resonance imaging. *Neurobiol. Dis.* **2002,** *11*, 315-329.

[79] Poduslo, J. F.; Curran, G. L.; Peterson, J. A.; McCormick, D. J.; Fauq, A. H.; Khan, M. A.; Wengenack, T. M. Design and chemical synthesis of a magnetic resonance contrast agent with enhanced *in vitro* binding, high blood-brain barrier permeability, and *in vivo* targeting to Alzheimer's disease amyloid plaques. *Biochemistry* **2004,** *43*, 6064-6075.

[80] Higuchi, M.; Iwata, N.; Matsuba, Y.; Sato, K.; Sasamoto, K.; Saido, T. C. 19F and 1H MRI detection of amyloid beta plaques *in vivo*. *Nat. Neurosci.* **2005,** *8*, 527-533.

[81] Hintersteiner, M.; Enz, A.; Frey, P.; Jaton, A. L.; Kinzy, W.; Kneuer, R.; Neumann, U.; Rudin, M.; Staufenbiel, M.; Stoeckli, M.; Wiederhold, K. H.; Gremlich, H. U. *In vivo* detection of amyloid-beta deposits by near-infrared imaging using an oxazine-derivative probe. *Nat. Biotechnol.* **2005,** *23*, 577-583.

[82] Ingelsson, M.; Fukumoto, H.; Newell, K. L.; Growdon, J. H.; Hedley-Whyte, E. T.; Frosch, M. P.; Albert, M. S.; Hyman, B. T.; Irizarry, M. C. Early Abeta accumulation and progressive synaptic loss, gliosis, and tangle formation in AD brain. *Neurology* **2004,** *62*, 925-931.

[83] Eckelman, W. C.; Kilbourn, M. R.; Mathis, C. A. Discussion of targeting proteins *in vivo*: *in vitro* guidelines. *Nucl. Med. Biol.* **2006,** *33*, 449-451.

[84] Mathis, C. A.; Wang, Y. M.; Holt, D. P.; Huang, G. F.; Debnath, M. L.; Klunk, W. E. Synthesis and evaluation of C-11-labeled 6-substituted 2-arylbenzothiazoles as amyloid imaging agents. *J. Med. Chem.* **2003,** *46*, 2740-2754.

[85] Pardridge, W. M. The blood-brain barrier: bottleneck in brain drug development. *NeuroRx* **2005,** *2*, 3-14.

[86] Eckelman, W. C.; Mathis, C. A. Targeting proteins *in vivo*: *in vitro* guidelines. *Nucl. Med. Biol.* **2006,** *33*, 161-164.

[87] Waterhouse, R. N. Determination of lipophilicity and its use as a predictor of blood-brain barrier penetration of molecular imaging agents. *Mol. Imaging Biol.* **2003,** *5*, 376-389.

[88] Vera, D. R.; Eckelman, W. C. Receptor 1980 and Receptor 2000: twenty years of progress in receptor-binding radiotracers. *Nucl. Med. Biol.* **2001,** *28*, 475-476.

[89] Fumita, M.; Innis, R. B. *In Vivo* Molecular Imaging: Ligand Development and Research Applications. In *Neuropsychopharmacology: The Fifth Generation of Progress.*, Davis, K. L.; Charney, D.; Coyle, J. T.; Nemeroff, C.; Eds.; American College of Neuropsychopharmacology: **2002**; Chapter 31, pp. 411-425.

[90] Lee, H. J.; Zhang, Y.; Zhu, C.; Duff, K.; Pardridge, W. M. Imaging brain amyloid of Alzheimer disease *in vivo* in transgenic mice with an Abeta peptide radiopharmaceutical. *J. Cereb. Blood Flow Metab.* **2002,** *22*, 223-231.

[91] Kurihara, A.; Pardridge, W. M. Abeta(1-40) peptide radiopharmaceuticals for brain amyloid imaging: (111)In chelation, conjugation to poly(ethylene glycol)-biotin linkers, and autoradiography with Alzheimer's disease brain sections. *Bioconjug. Chem.* **2000,** *11*, 380-386.

[92] Marshall, J. R.; Stimson, E. R.; Ghilardi, J. R.; Vinters, H. V.; Mantyh, P. W.; Maggio, J. E. Noninvasive imaging of peripherally injected Alzheimer's disease type synthetic A beta amyloid *in vivo*. *Bioconjug. Chem.* **2002,** *13*, 276-284.

[93] Friedland, R. P.; Majocha, R. E.; Reno, J. M.; Lyle, L. R.; Marotta, C. A. Development of an anti-A beta monoclonal antibody for *in vivo* imaging of amyloid angiopathy in Alzheimer's disease. *Mol. Neurobiol.* **1994,** *9*, 107-113.

[94] Wengenack, T. M.; Curran, G. L.; Poduslo, J. F. Targeting alzheimer amyloid plaques *in vivo*. *Nat. Biotechnol.* **2000,** *18*, 868-872.

[95] Klunk, W. E.; Pettegrew, J. W.; Abraham, D. J. Quantitative evaluation of congo red binding to amyloid-like proteins with a beta-pleated sheet conformation. *J. Histochem. Cytochem.* **1989,** *37*, 1273-1281.

[96] Klunk, W. E.; Debnath, M. L.; Koros, A. M.; Pettegrew, J. W. Chrysamine-G, a lipophilic analogue of Congo red, inhibits A beta-induced toxicity in PC12 cells. *Life Sci.* **1998,** *63*, 1807-1814.

[97] Klunk, W. E.; Debnath, M. L.; Pettegrew, J. W. Chrysamine-G binding to Alzheimer and control brain: autopsy study of a new amyloid probe. *Neurobiol. Aging* **1995,** *16*, 541-548.

[98] Klunk, W. E.; Bacskai, B. J.; Mathis, C. A.; Kajdasz, S. T.; McLellan, M. E.; Frosch, M. P.; Debnath, M. L.; Holt, D. P.; Wang, Y. M.; Hyman, B. T. Imaging A beta plaques in living transgenic mice with multiphoton microscopy and methoxy-X04, a systemically administered Congo red derivative. *J. Neuropathol. Exp. Neurol.* **2002,** *61*, 797-805.

[99] Skovronsky, D. M.; Zhang, B.; Kung, M. P.; Kung, H. F.; Trojanowski, J. Q.; Lee, V. M. *In vivo* detection of amyloid plaques in a mouse model of Alzheimer's disease. *Proc. Natl. Acad. Sci. U. S. A.* **2000,** *97*, 7609-7614.

[100] Zhuang, Z. P.; Kung, M. P.; Hou, C.; Skovronsky, D. M.; Gur, T. L.; Plossl, K.; Trojanowski, J. Q.; Lee, V. M. Y.; Kung, H. F. Radioiodinated styrylbenzenes and thioflavins as probes for amyloid aggregates. *J. Med. Chem.* **2001,** *44*, 1905-1914.

[101] Kumar, P.; Zheng, W. Z.; McQuarrie, S. A.; Jhamandas, J. H.; Wiebe, L. I. F-18-FESB: synthesis and automated radiofluorination of a novel F-18-labeled pet tracer for beta-amyloid plaques. *J. Label. Compd. Radiopharm.* **2005,** *48*, 983-996.

[102] LeVine, H., 3rd. Thioflavine T interaction with synthetic Alzheimer's disease beta-amyloid peptides: detection of amyloid aggregation in solution. *Protein Sci.* **1993,** *2*, 404-410.

[103] Mathis, C. A.; Bacskai, B. J.; Kajdasz, S. T.; McLellan, M. E.; Frosch, M. P.; Hyman, B. T.; Holt, D. P.; Wang, Y. M.; Huang, G. F.; Debnath, M. L.; Klunk, W. E. A lipophilic thioflavin-T derivative for positron emission tomography (PET) Imaging of amyloid in brain. *Bioorg. Med. Chem. Lett.* **2002,** *12*, 295-298.

[104] Klunk, W. E.; Wang, Y. M.; Huang, G. F.; Debnath, M. L.; Holt, D. P.; Mathis, C. A. Uncharged thioflavin-T derivatives bind to amyloid-beta protein with high affinity and readily enter the brain. *Life Sci.* **2001,** *69*, 1471-1484.

[105] Wang, Y.; Mathis, C. A.; Huang, G. F.; Debnath, M. L.; Holt, D. P.; Shao, L.; Klunk, W. E. Effects of lipophilicity on the affinity and nonspecific binding of iodinated benzothiazole derivatives. *J. Mol. Neurosci.* **2003,** *20*, 255-260.

[106] Klunk, W. E.; Lopresti, B. J.; Ikonomovic, M. D.; Lefterov, I. M.; Koldamova, R. P.; Abrahamson, E. E.; Debnath, M. L.; Holt, D. P.; Huang, G. F.; Shao, L.; DeKosky, S. T.; Price, J. C.; Mathis, C. A. Binding of the positron emission tomography tracer Pittsburgh compound-B reflects the amount of amyloid-beta in Alzheimer's disease brain but not in transgenic mouse brain. *J. Neurosci.* **2005,** *25*, 10598-10606.

[107] Zhuang, Z. P.; Kung, M. P.; Hou, C.; Plossl, K.; Skovronsky, D.; Gur, T. L.; Trojanowski, J. Q.; Lee, V. M. Y.; Kung, H. F. IBOX(2-(4'-dimethylaminophenyl)-6-iodobenzoxazole): a ligand for imaging amyloid plaques in the brain. *Nucl. Med. Biol.* **2001,** *28*, 887-894.

[108] Ono, M.; Kawashima, H.; Nonaka, A.; Kawai, T.; Haratake, M.; Mori, H.; Kung, M. P.; Kung, H. F.; Saji, H.; Nakayama, M. Novel benzofuran derivatives for PET imaging of beta-amyloid plaques in Alzheimer's disease brains. *J. Med. Chem.* **2006,** *49*, 2725-2730.

[109] Ono, M.; Kung, M. P.; Hou, C.; Kung, H. F. Benzofuran derivatives as A beta-aggregate-specific imaging agents for Alzheimer's disease. *Nucl. Med. Biol.* **2002,** *29*, 633-642.

[110] Kung, M. P.; Hou, C.; Zhuang, Z. P.; Zhang, B.; Skovronsky, D.; Trojanowski, J. Q.; Lee, V. M. Y.; Kung, H. F. IMPY: an improved thioflavin-T derivative for *in vivo* labeling of beta-amyloid plaques. *Brain Res.* **2002,** *956*, 202-210.

[111] Zhuang, Z. P.; Kung, M. P.; Wilson, A.; Lee, C. W.; Plossl, K.; Hou, C.; Holtzman, D. M.; Kung, H. F. Structure-activity relationship of imidazo 1,2-alpha pyridines as ligands for detecting beta-amyloid plaques in the brain. *J. Med. Chem.* **2003,** *46*, 237-243.

[112] Kung, M. P.; Hou, C.; Zhuang, Z. P.; Cross, A. J.; Maier, D. L.; Kung, H. F. Characterization of IMPY as a potential imaging agent for beta-amyloid plaques in double transgenic PSAPP mice. *Eur. J. Nucl. Med. Mol. Imaging* **2004,** *31*, 1136-1145.

[113] Newberg, A. B.; Wintering, N. A.; Plossl, K.; Hochold, J.; Stabin, M. G.; Watson, M.; Skovronsky, D.; Clark, C. M.; Kung, M. P.; Kung, H. F. Safety, biodistribution, and dosimetry of I-123-IMPY: a novel amyloid plaque-imaging agent for the diagnosis of Alzheimer's disease. *J. Nucl. Med.* **2006,** *47*, 748-754.

[114] Kung, M. P.; Hou, C.; Zhuang, Z. P.; Skovronsky, D.; Kung, H. F. Binding of two potential imaging agents targeting amyloid plaques in postmortem brain tissues of patients with Alzheimer's disease. *Brain Res.* **2004,** *1025*, 98-105.

[115] Serdons, K. Comparative Evaluation of 2-(4'-[18F]fluorophenyl)-1,3-benzothiazole and [11C]6-OH-BTA-1 as Amyloid Imaging Agents. *Eur. J. Nucl. Med. Mol. Imaging* **2005,** *32*, S43.

[116] Serdons, K. Evaluation of a new potential amyloid imaging agent: 6-methyl-2-(4'-[18F]fluorophenyl)-1,3-benzothiazole. *Eur. J. Nucl. Med. Mol. Imaging* **2006,** *33*, S218.

[117] Chang, Y. S.; Jeong, J. M.; Lee, Y. S.; Kim, H. W.; Ganesha, R. B.; Kim, Y. J.; Lee, D. S.; Chung, J. K.; Lee, M. C. Synthesis and evaluation of benzothiophene derivatives as ligands for imaging beta-amyloid plaques in Alzheimer's disease. *Nucl. Med. Biol.* **2006,** *33*, 811-820.

[118] Cai, L.; Chin, F. T.; Pike, V. W.; Toyama, H.; Liow, J. S.; Zoghbi, S. S.; Modell, K.; Briard, E.; Shetty, H. U.; Sinclair, K.; Donohue, S.; Tipre, D.; Kung, M. P.; Dagostin, C.; Widdowson, D. A.; Green, M.; Gao, W.; Herman, M. M.; Ichise, M.; Innis, R. B. Synthesis and evaluation of two 18F-labeled 6-iodo-2-(4'-N,N-dimethylamino)phenylimidazo[1,2-a]pyridine derivatives as prospective radioligands for beta-amyloid in Alzheimer's disease. *J. Med. Chem.* **2004,** *47*, 2208-2218.

[119] Zeng, F.; Southerland, J. A.; Voll, R. J.; Votaw, J. R.; Williams, L.; Ciliax, B. J.; Levey, A. I.; Goodman, M. M. Synthesis and evaluation of two 18F-labeled imidazo[1,2-a]pyridine analogues as potential agents for imaging beta-amyloid in Alzheimer's disease. *Bioorg. Med. Chem. Lett.* **2006,** *16*, 3015-3018.

[120] Kung, H. F.; Lee, C. W.; Zhuang, Z. P.; Kung, M. P.; Hou, C.; Plossl, K. Novel stilbenes as probes for amyloid plaques. *J. Am. Chem. Soc.* **2001,** *123*, 12740-12741.

[121] Kung, H. F. Imaging of Aβ plaques in the brain of Alzheimer's disease. *Int. Congress Series* **2004,** *1264*, 3-9.

[122] Ono, M.; Wilson, A.; Nobrega, J.; Westaway, D.; Verhoeff, P.; Zhuang, Z. P.; Kung, M. P.; Kung, H. F. C-11-labeled stilbene derivatives as A beta-aggregate-specific PET imaging agents for Alzheimer's disease. *Nucl. Med. Biol.* **2003,** *30*, 565-571.

[123] Zhang, W.; Oya, S.; Kung, M. P.; Hou, C.; Maier, D. L.; Kung, H. F. F-18 Stilbenes as PET imaging agents for detecting beta-amyloid plaques in the brain. *J. Med. Chem.* **2005,** *48*, 5980-5988.

[124] Zhang, W.; Oya, S.; Kung, M. P.; Hou, C.; Maier, D. L.; Kung, H. F. F-18 polyethyleneglycol stilbenes as PET imaging agents targeting A beta aggregates in the brain. *Nucl. Med. Biol.* **2005,** *32*, 799-809.

[125] Ono, M.; Haratake, M.; Nakayama, M.; Kaneko, Y.; Kawabata, K.; Mori, H.; Kung, M. P.; Kung, H. F. Synthesis and biological evaluation of (E)-3-styrylpyridine derivatives as amyloid imaging agents for Alzheimer's disease. *Nucl. Med. Biol.* **2005,** *32*, 329-335.

[126] Stephenson, K. A.; Chandra, R.; Zhuang, Z. P.; Hou, C.; Oya, S.; Kung, M. P.; Kung, H. F. Fluoro-pegylated (FPEG) imaging agents targeting Abeta aggregates. *Bioconjug. Chem.* **2007,** *18*, 238-246.

[127] Zhang, W.; Kung, M. P.; Oya, S.; Hou, C.; Kung, H. F. 18F-labeled styrylpyridines as PET agents for amyloid plaque imaging. *Nucl. Med. Biol.* **2007,** *34*, 89-97.

[128] Shimadzu, H.; Suemoto, T.; Suzuki, M.; Shiomitsu, T.; Okamura, N.; Kudo, Y.; Sawada, T. Novel probes for imaging amyloid-beta: F-18 and C-11 labeling of 2-(4-aminostyryl)benzoxazole derivatives. *J. Label. Compd. Radiopharm.* **2004,** *47*, 181-190.

[129] Okamura, N.; Suemoto, T.; Shiomitsu, T.; Suzuki, M.; Shimadzu, H.; Akatsu, H.; Yamamoto, T.; Arai, H.; Sasaki, H.; Yanai, K.; Staufenbiel, M.; Kudo, Y.; Sawada, T. A novel imaging probe for *in vivo* detection of neuritic and diffuse amyloid plaques in the brain. *J. Mol. Neurosci.* **2004,** *24*, 247-255.

[130] Okamura, N.; Suemoto, T.; Shimadzu, H.; Suzuki, M.; Shiomitsu, T.; Akatsu, H.; Yamamoto, T.; Staufenbiel, M.; Yanai, K.; Arai, H.; Sasaki, H.; Kudo, Y.; Sawada, T. Styrylbenzoxazole derivatives for *in vivo* imaging of amyloid plaques in the brain. *J. Neurosci.* **2004,** *24*, 2535-2541.

[131] Okamura, N.; Suemoto, T.; Furumoto, S.; Suzuki, M.; Shimadzu, H.; Akatsu, H.; Yamamoto, T.; Fujiwara, H.; Nemoto, M.; Maruyama, M.; Arai, H.; Yanai, K.; Sawada, T.; Kudo, Y. Quinoline and benzimidazole derivatives: candidate probes for *in vivo* imaging of tau pathology in Alzheimer's disease. *J. Neurosci.* **2005,** *25*, 10857-10862.

[132] Kudo, Y.; Okamura, N.; Furumoto, S.; Tashiro, M.; Furukawa, K.; Maruyama, M.; Itoh, M.; Iwata, R.; Yanai, K.; Arai, H. 2-[2-(2-Dimethylaminothiazol-5-yl)ethenyl]-6-[2-fluroroethoxy]benzoxazole (BF227): A novel PET imaging agent for *in vivo* detection of dense amyloid plaques in Alzheimer's disease patients. *J. Nucl. Med.* **2007,** *48*, 553-561.

[133] Furumoto, S.; Okamura, N.; Ishikawa, Y.; Tashiro, M.; Kato, M.; Funaki, Y.; Maruyama, M.; Akatsu, H.; Suemoto, T.; Yamamoto, T.; Arai, H.; Sawada, T.; Iwata, R.; Yanai, K.; Kudo, Y. [11C]BF227: A New 11C-Labeled 2-Ethenylbenzoxazole Derivative for Amyloid-β Plaques Imaging. *Eur. J. Nucl. Med. Mol. Imaging* **2005,** *32*, S161.

[134] Jacobson, A.; Petric, A.; Hogenkamp, D.; Sinur, A.; Barrio, J. R. 1,1-Dicyano-2-[6-(Dimethylamino)Naphthalen-2-YI]Propene (Ddnp) - a Solvent Polarity and Viscosity Sensitive Fluorophore for Fluorescence Microscopy. *J. Am. Chem. Soc.* **1996,** *118*, 5572-5579.

[135] Liu, J.; Kepe, V.; Zabjek, A.; Petric, A.; Padgett, H. C.; Satyamurthy, N.; Barrio, J. R. High-yield, automated radiosynthesis of 2-(1-{6-[(2-[18F] fluoroethyl)(methyl)amino]-2-naphthyl}ethylidene)malononi trile ([18F] FDDNP) ready for animal or human administration. *Mol. Imaging Biol.* **2007,** *9*, 6-16.

[136] Agdeppa, E. D.; Kepe, V.; Liu, J.; Flores-Torres, S.; Satyamurthy, N.; Petric, A.; Cole, G. M.; Small, G. W.; Huang, S. C.; Barrio, J. R. Binding characteristics of radiofluorinated 6-dialkylamino-2-naphthylethylidene derivatives as positron emission tomography imaging probes for beta-amyloid plaques in Alzheimer's disease. *J. Neurosci.* **2001,** *21*, RC189.

[137] Agdeppa, E. D.; Kepe, V.; Liu, J.; Small, G. W.; Huang, S. C.; Petric, A.; Satyamurthy, N.; Barrio, J. R. 2-Dialkylamino-6-acylmalononitrile substituted naphthalenes (DDNP analogs): novel diagnostic and therapeutic tools in Alzheimer's disease. *Mol. Imaging Biol.* **2003,** *5*, 404-417.

[138] Agdeppa, E. D.; Kepe, V.; Petric, A.; Satyamurthy, N.; Liu, J.; Huang, S. C.; Small, G. W.; Cole, G. M.; Barrio, J. R. *In vitro* detection of (S)-naproxen and ibuprofen binding to plaques in the Alzheimer's brain using the positron emission tomography molecular imaging probe 2-(1-{6-(2[F-18 fluoroethyl) (methyl)amino]-2-naphthyl}ethylidene) malononitrile. *Neurosci.* **2003,** *117*, 723-730.

[139] Kung, H. F.; Kung, M. P.; Zhuang, Z. P.; Hou, C.; Lee, C. W.; Plossl, K.; Zhuang, B.; Skovronsky, D. M.; Lee, V. M.; Trojanowski, J. Q. Iodinated tracers for imaging amyloid plaques in the brain. *Mol. Imaging Biol.* **2003,** *5*, 418-426.

[140] Lee, C. W.; Kung, M. P.; Hou, C.; Kung, H. F. Dimethylamino-fluorenes: ligands for detecting beta-amyloid plaques in the brain. *Nucl. Med. Biol.* **2003,** *30*, 573-580.

[141] Chandra, R.; Kung, M. P.; Kung, H. F. Design, synthesis, and structure-activity relationship of novel thiophene derivatives for beta-amyloid plaque imaging. *Bioorg. Med. Chem. Lett.* **2006,** *16*, 1350-1352.

[142] Zhuang, Z. P.; Kung, M. P.; Kung, H. F. Synthesis of biphenyltrienes as probes for beta-amyloid plaques. *J. Med. Chem.* **2006,** *49*, 2841-2844.

[143] Shimadzu, H.; Suemoto, T.; Suzuki, M.; Shiomitsu, T.; Okamura, N.; Kudo, Y. A.; Sawada, T. A novel probe for imaging amyloid-beta: Synthesis of F-18 labelled BF-108, an Acridine Orange analog. *J. Label. Compd. Radiopharm.* **2003,** *46*, 765-772.

[144] Suemoto, T.; Okamura, N.; Shiomitsu, T.; Suzuki, M.; Shimadzu, H.; Akatsu, H.; Yamamoto, T.; Kudo, Y.; Sawada, T. *In vivo* labeling of amyloid with BF-108. *Neurosci. Res.* **2004,** *48*, 65-74.

[145] Ono, K.; Hamaguchi, T.; Naiki, H.; Yamada, M. Anti-amyloidogenic effects of antioxidants: implications for the prevention and therapeutics of Alzheimer's disease. *Biochim. Biophys. Acta* **2006,** *1762*, 575-586.

[146] Ono, K.; Hasegawa, K.; Naiki, H.; Yamada, M. Curcumin has potent anti-amyloidogenic effects for Alzheimer's beta-amyloid fibrils *in vitro*. *J. Neurosci. Res.* **2004,** *75*, 742-750.

[147] Ono, K.; Yoshiike, Y.; Takashima, A.; Hasegawa, K.; Naiki, H.; Yamada, M. Potent anti-amyloidogenic and fibril-destabilizing effects of polyphenols *in vitro*: implications for the prevention and therapeutics of Alzheimer's disease. *J. Neurochem.* **2003,** *87*, 172-181.

[148] Yang, F.; Lim, G. P.; Begum, A. N.; Ubeda, O. J.; Simmons, M. R.; Ambegaokar, S. S.; Chen, P. P.; Kayed, R.; Glabe, C. G.; Frautschy, S. A.; Cole, G. M. Curcumin inhibits formation of amyloid beta oligomers and fibrils, binds plaques, and reduces amyloid *in vivo*. *J. Biol. Chem.* **2005,** *280*, 5892-5901.

[149] Ono, M.; Yoshida, N.; Ishibashi, K.; Haratake, M.; Arano, Y.; Mori, H.; Nakayama, M. Radioiodinated flavones for *in vivo* imaging of beta-amyloid plaques in the brain. *J. Med. Chem.* **2005,** *48*, 7253-7260.

[150] Ono, M.; Maya, Y.; Haratake, M.; Nakayama, M. Synthesis and characterization of styrylchromone derivatives as beta-amyloid imaging agents. *Bioorg. Med. Chem.* **2007,** *15*, 444-450.

[151] Ryu, E. K.; Choe, Y. S.; Lee, K. H.; Choi, Y.; Kim, B. T. Curcumin and dehydrozingerone derivatives: synthesis, radiolabeling, and evaluation for beta-amyloid plaque imaging. *J. Med. Chem.* **2006,** *49*, 6111-6119.

[152] Klunk, W. E.; Engler, H.; Nordberg, A.; Wang, Y. M.; Blomqvist, G.; Holt, D. P.; Bergstrom, M.; Savitcheva, I.; Huang, G. F.; Estrada, S.; Ausen, B.; Debnath, M. L.; Barletta, J.; Price, J. C.; Sandell, J.; Lopresti, B. J.; Wall, A.; Koivisto, P.; Antoni, G.; Mathis, C. A.; Langstrom, B. Imaging brain amyloid in Alzheimer's disease with Pittsburgh Compound-B. *Ann. Neurol.* **2004,** *55*, 306-319.

[153] Arnold, S. E.; Hyman, B. T.; Flory, J.; Damasio, A. R.; Van Hoesen, G. W. The topographical and neuroanatomical distribution of neurofibrillary tangles and neuritic plaques in the cerebral cortex of patients with Alzheimer's disease. *Cereb. Cortex* **1991,** *1*, 103-116.

[154] Thal, D. R.; Rub, U.; Orantes, M.; Braak, H. Phases of A beta-deposition in the human brain and its relevance for the development of AD. *Neurology* **2002,** *58*, 1791-1800.

[155] Price, J. C.; Klunk, W. E.; Lopresti, B. J.; Lu, X.; Hoge, J. A.; Ziolko, S. K.; Holt, D. P.; Meltzer, C. C.; DeKosky, S. T.; Mathis, C. A. Kinetic modeling of amyloid binding in humans using PET imaging and Pittsburgh Compound-B. *J. Cereb. Blood Flow Metab.* **2005,** *25*, 1528-1547.

[156] Lopresti, B. J.; Klunk, W. E.; Mathis, C. A.; Hoge, J. A.; Ziolko, S. K.; Lu, X. L.; Meltzer, C. C.; Schimmel, K.; Tsopelas, N. D.; DeKosky, S. T.; Price, J. C. Simplified quantification of Pittsburgh compound B amyloid imaging PET studies: A comparative analysis. *J. Nucl. Med.* **2005,** *46*, 1959-1972.

[157] Ziolko, S. K.; Weissfeld, L. A.; Klunk, W. E.; Mathis, C. A.; Hoge, J. A.; Lopresti, B. J.; DeKosky, S. T.; Price, J. C. Evaluation of voxel-based methods for the statistical analysis of PIB PET amyloid imaging studies in Alzheimer's disease. *Neuroimage* **2006,** *33*, 94-102.

[158] Buckner, R. L.; Snyder, A. Z.; Shannon, B. J.; LaRossa, G.; Sachs, R.; Fotenos, A. F.; Sheline, Y. I.; Klunk, W. E.; Mathis, C. A.; Morris, J. C.; Mintun, M. A. Molecular, structural, and functional characterization of Alzheimer's disease: Evidence for a relationship between default activity, amyloid, and memory. *J. Neurosci.* **2005,** *25*, 7709-7717.

[159] Engler, H.; Forsberg, A.; Almkvist, O.; Blomquist, G.; Larsson, E.; Savitcheva, I.; Wall, A.; Ringheim, A.; Langstrom, B.; Nordberg, A. Two-year follow-up of amyloid deposition in patients with Alzheimer's disease. *Brain* **2006,** *129*, 2856-2866.

[160] Archer, H. A.; Edison, P.; Brooks, D. J.; Barnes, J.; Frost, C.; Yeatman, T.; Fox, N. C.; Rossor, M. N. Amyloid load and cerebral atrophy in Alzheimer's disease: an 11C-PIB positron emission tomography study. *Ann. Neurol.* **2006,** *60*, 145-147.

[161] Edison, P.; Archer, H. A.; Hinz, R.; Hammers, A.; Pavese, N.; Tai, Y. F.; Hotton, G.; Cutler, D.; Fox, N.; Kennedy, A.; Rossor, M.; Brooks, D. J. Amyloid, hypometabolism, and cognition in Alzheimer disease: an [11C]PIB and [18F]FDG PET study. *Neurology* **2007,** *68*, 501-508.

[162] Fagan, A. M.; Mintun, M. A.; Mach, R. H.; Lee, S. Y.; Dence, C. S.; Shah, A. R.; LaRossa, G. N.; Spinner, M. L.; Klunk, W. E.; Mathis, C. A.; DeKosky, S. T.; Morris, J. C.; Holtzman, D. M. Inverse relation between *in vivo* amyloid imaging load and cerebrospinal fluid A beta(42) in humans. *Ann. Neurol.* **2006,** *59*, 512-519.

[163] Mintun, M. A.; Larossa, G. N.; Sheline, Y. I.; Dence, C. S.; Lee, S. Y.; Mach, R. H.; Klunk, W. E.; Mathis, C. A.; DeKosky, S. T.; Morris, J. C. [11C]PIB in a nondemented population: potential antecedent marker of Alzheimer disease. *Neurology* **2006,** *67*, 446-452.

[164] Verhoeff, N.; Wilson, A. A.; Takeshita, S.; Trop, L.; Hussey, D.; Singh, K.; Kung, H. F.; Kung, M. P.; Houle, S. In-vivo imaging of Alzheimer disease beta-amyloid with. *Am. J. Geriatr. Psychiatry* **2004,** *12*, 584-595.

[165] Shoghi-Jadid, K.; Small, G. W.; Agdeppa, E. D.; Kepe, V.; Ercoli, L. M.; Siddarth, P.; Read, S.; Satyamurthy, N.; Petric, A.; Huang, S. C.; Barrio, J. R. Localization of neurofibrillary tangles and beta-amyloid plaques in the brains of living patients with Alzheimer disease. *Am. J. Geriatr. Psychiatry* **2002,** *10*, 24-35.

[166] Barrio, J. R.; Kepe, V.; Satyamurthy, N.; Huang, S.-C.; Small, G. W. Brain pathology and neuronal losses in the living brain of Alzheimer's patients. *Int. Congress Series* **2006,** *1290*, 150-155.

[167] Small, G. W.; Kepe, V.; Ercoli, L. M.; Siddarth, P.; Bookheimer, S. Y.; Miller, K. J.; Lavretsky, H.; Burggren, A. C.; Cole, G. M.; Vinters, H. V.; Thompson, P. M.; Huang, S. C.; Satyamurthy, N.; Phelps, M. E.; Barrio, J. R. PET of brain amyloid and tau in mild cognitive impairment. *N. Engl. J. Med.* **2006,** *355*, 2652-2663.

Received: February 22, 2007 Accepted: March 20, 2007

Geriatr Gerontol Int 2007; 7: 393–400

ORIGINAL ARTICLE: BIOLOGY

Binding and safety profile of novel benzoxazole derivative for *in vivo* imaging of amyloid deposits in Alzheimer's disease

Nobuyuki Okamura,[1] Shozo Furumoto,[2] Yoshihito Funaki,[3] Takahiro Suemoto,[4] Motohisa Kato,[1] Yoichi Ishikawa,[3] Satoshi Ito,[1] Hiroyasu Akatsu,[5] Takayuki Yamamoto,[5] Tohru Sawada,[4] Hiroyuki Arai,[6] Yukitsuka Kudo[2] and Kazuhiko Yanai[1]

[1]Department of Pharmacology, Tohoku University Graduate School of Medicine, [2]Tohoku University Biomedical Engineering Research Organization (TUBERO), [3]Division of Radiopharmaceutical Chemistry, Cyclotron and Radioisotope Center, Tohoku University, [6]Center for Asian Traditional Medicine, Department of Geriatrics and Gerontology, Tohoku University School of Medicine, Sendai, [4]BF Research Institute, Osaka, and [5]Fukushimura Hospital, Toyohashi, Japan

Background: *In vivo* detection of amyloid deposits in the brain is potentially useful for early diagnosis of Alzheimer's disease (AD) and tracking the efficacy of anti-amyloid therapy.

Methods: To develop an amyloid-binding agent for positron emission tomography, we screened over 2600 compounds.

Results: We found benzoxazole derivatives as candidate compounds for *in vivo* amyloid imaging probes. One of these agents, 2-(2-[2-dimethylaminothiazol-5-yl]ethenyl)-6-(2-[fluoro]ethoxy)benzoxazole (BF-227), displays high binding affinity to Aβ fibrils. BF-227 binding increased linearly with increasing Aβ fibril formation. In temporal and hippocampal AD brain sections, BF-227 selectively bound to amyloid plaques. In contrast, no staining was evident in the cerebellum. Compared with the previously reported compound BF-168, ^{18}F-labeled BF-227 displayed selective *in vivo* labeling of amyloid fibrils and rapid washout from white matter areas in an Aβ-injected rat model. An acute and subacute toxicity study of BF-227 indicated sufficient safety for clinical use as a positron emission tomography probe.

Conclusions: These findings suggest that BF-227 is feasible as an *in vivo* imaging probe of amyloid deposits in AD patients.

Keywords: Alzheimer's disease, amyloid, positron emission tomography, senile plaques.

Introduction

Progressive deposition of senile plaques (SP) and neurofibrillary tangles (NFT) is a critical event in the pathogenesis of Alzheimer's disease (AD). These lesions precede the presentation of clinical symptoms of dementia.[1] For early or presymptomatic diagnosis of AD, non-invasive detection of these lesions using positron emission tomography (PET) is a potentially

Accepted for publication 22 August 2007.

Correspondence: Dr Nobuyuki Okamura MD PhD, Department of Pharmacology, Tohoku University Graduate School of Medicine, 2-1 Seiryo-machi, Aoba-ku, Sendai 980-8575, Japan. Email: oka@mail.tains.tohoku.ac.jp

doi: 10.1111/j.1447-0594.2007.00430.x

useful technique.[2] To achieve successful *in vivo* imaging using PET, sensitive and selective contrast agents to these lesions are needed. Congo red and thioflavin T have represented attractive lead compounds as developing amyloid-imaging agents, because these compounds selectively bind to β-pleated sheet structures and are commonly used for histochemical staining of SP. However, the permeability of these compounds through the blood–brain barrier (BBB) is extremely limited.[3] The chemical structure must thus be optimized to provide appropriate lipophilicity without changing the binding properties to amyloid. Thioflavin T derivatives without any positive charge show high permeability of the BBB. One of these compounds, 6OH-BTA-1 (PIB), has been applied in a human PET study and enabled successful detection of early AD patients.[4] Another compound, 2-(1-[6-{<2-fluoroethyl><methyl>amino}-2-naphthyl]ethylidene) malononitrile (FDDNP), is extremely lipophilic and can easily penetrate the BBB, and specifically binds to both SP and NFT in AD brain sections.[5] After i.v. injection of FDDNP, greater accumulation was observed in SP- and NFT-rich areas of the human brain.[6] Although validation is still required as to whether retention of these agents in the neocortex truly reflects levels of amyloid deposition, such findings suggest the potential usefulness of this technique for early diagnosis of AD.

We have previously demonstrated a novel series of compounds including 6-(2-fluoroethoxy)-2-(2-[4-methylaminophenyl]ethenyl)benzoxazole (BF-168) and (2-[4-methylaminophenyl]ethenyl)-5-fluorobenzoxazole (BF-145) as promising candidates for *in vivo* imaging probes of SP.[7–9] These benzoxazole derivatives demonstrate high binding affinity for Aβ aggregates and high BBB permeability, suggesting potential utility as *in vivo* amyloid-binding agents. However, for the application of these compounds to clinical PET studies, the pharmacokinetic properties and pharmacological safety of these molecules requires improvement. This study describes the characterization of an optimized benzoxazole derivative, 2-(2-[2-dimethylaminothiazol-5-yl]ethenyl)-6-(2-[fluoro]ethoxy) benzoxazole (BF-227), as a candidate *in vivo* amyloid-imaging agent in humans.

Methods

Preparation of the compounds

BF-168, BF-227 (Fig. 1) and the precursor compounds for ^{18}F-labeled agents were custom-synthesized by Tanabe R & D Service (Osaka, Japan). Synthesis of (^{18}F)BF-168 was performed by reacting 2-(4-methylaminophenyl)-6-(2-tosyloxyethoxy) benzoxazole (Tanabe R & D Service) with (^{18}F)KF and Kryptofix 222 (Merck, Darmstadt, Germany) in acetonitrile at 80°C for 20 min, as described previously.[8] Radiosynthesis of (^{18}F)BF-227 was performed using the same method. After subsequent high-performance liquid chromatography (HPLC) purification, ^{18}F-labeled compounds were obtained (Fig. 1). Details of the radiosynthetic methods will be described elsewhere.

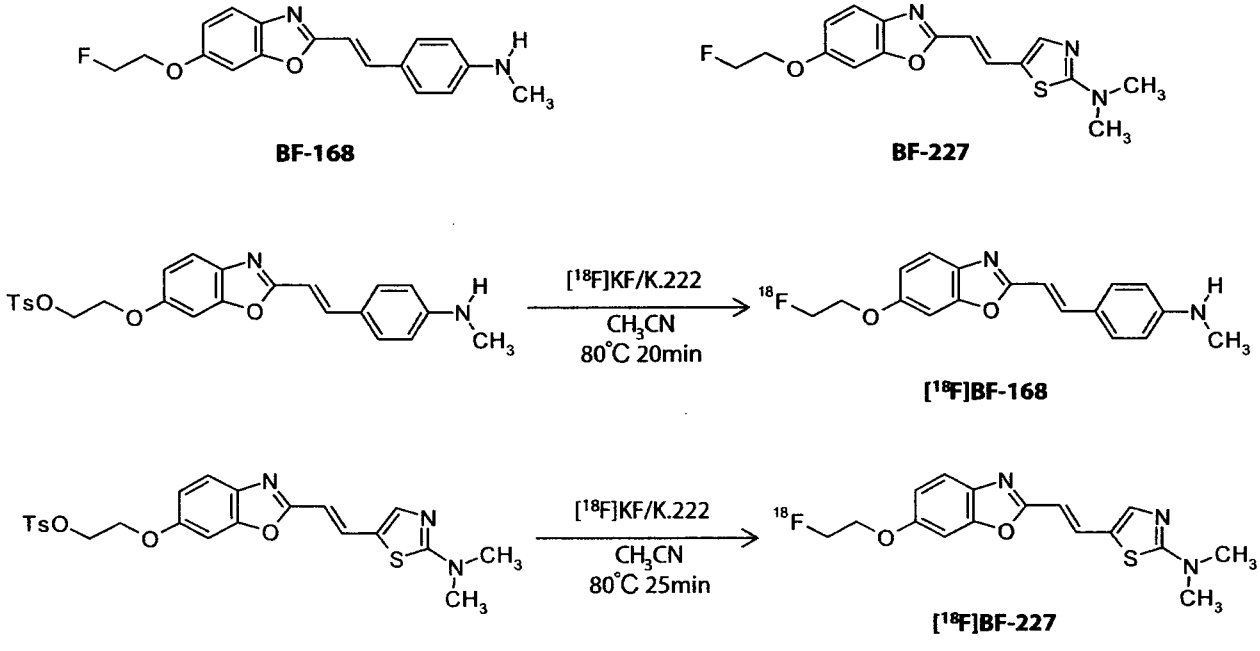

Figure 1 Chemical structures and radiosynthesis of BF-168 and BF-227.

In vitro *binding assays*

Binding affinities of the compounds for synthetic Aβ aggregates were examined as described previously.[7] Briefly, solid-form Aβ1–40 (Peptide Institute, Osaka, Japan) was dissolved in 10 mmol/L potassium phosphate buffer (pH 7.4) and incubated at 37°C for 72 h. The binding assay was performed by mixing aggregated Aβ1–40 with the appropriate concentration of ^{18}F-labeled BF-227, unlabeled BF-227 and dimethyl sulfoxide. After incubation for 10 min at room temperature, the binding mixture was filtered using a cell harvester (Model M-24; Brandel, Gaithersburg, MD, USA) and filters containing bound ^{18}F ligand were counted using a γ-counter. The dissociation constant (K_d) of BF-227 was determined by Scatchard analysis.

Fluorometric analysis of BF-227 binding with Aβ fibrils was performed using the following method. A total of 20 μmol/L of Aβ1–40 or Aβ1–42 (Peptide Institute) in 50 mmol/L of potassium phosphate buffer (pH 7.4) was incubated at 37°C on a Vibrax VXR shaker (IKA, Cincinnati, OH, USA) at 0.56 *g*. Before fluorometric analysis, Aβ solutions were sonicated for 3 min at 45 kHz using a VS-100III ultrasonic cleaner (Iuchi, Osaka, Japan). In fluorometry, Aβ1–40 and Aβ1–42 solutions at 0, 4, 8 and 24 h after the start of incubation were mixed with the same volume of BF-227 solution (5 μmol/L final concentration). After determination of the optimal excitation wavelength for the mixture of BF-227 and Aβ, fluorescence spectra were measured using a Gemini XS microplate spectrofluorometer (Molecular Devices, Sunnyvale, CA, USA). In addition, fluorescence spectra for the mixture of 5 μM BF-227 and different concentrations of Aβ1–40 or Aβ1–42 (0.15, 0.5 1.5, 2.5, 5 and 10 μmol/L final concentrations) at 96 h after incubation (fibrillar Aβ) were measured using the microplate spectrofluorometer. The same measurements were also performed using Aβ1–40 and Aβ1–42 with no incubation (non-fibrillar Aβ). All measurements were performed in triplicate.

Neuropathological staining

Postmortem brain tissues from an autopsy-confirmed AD case (69-year-old man) were obtained from Fukushimura Hospital (Toyohashi, Japan). Experiments were performed under the regulations of the Ethics Committee of BF Research Institute. Serial sections (6-μm thick) from paraffin-embedded blocks of temporal cortex and cerebellum were prepared in xylene and ethanol. Before staining, quenching of autofluorescence was performed as described previously. Quenched tissue sections were immersed in 100 μmol/L of BF-227 solution for 10 min or 0.01% 1-bromo-2,5-bis(3-carboxy-4-hydroxystyryl)benzene (BSB) solution containing 50% ethanol for 30 min. Sections stained with BF-227 were then dipped briefly into water and rinsed in phosphate-buffered saline (PBS) for 60 min before coverslipping with Fluor Save Reagent (Calbiochem, La Jolla, CA, USA), and examined using an Eclipse E800 microscope (Nikon, Tokyo, Japan) equipped with a V-2A filter set (excitation 380–420 nm, dichroic mirror 430 nm, longpass filter 450 nm). Sections stained with BSB were dipped briefly in tap water and then in 50% ethanol, then washed in PBS for 60 min before coverslipping, followed by fluorescent microscopy using a BV-2A filter set (excitation 400–440 nm, dichroic mirror 455 nm, longpass filter 470 nm). In addition, adjacent sections were immunostained using monoclonal antibody (mAb) against Aβ (6F/3D; Dako A/S, Glostrup, Denmark). After pretreatment with 90% formic acid for 5 min, sections were immersed in blocking solution for 30 min and then incubated for 60 min at 37°C with 6F/3D at a dilution of 1:50. Following incubation, sections were processed by the avidin–biotin method using a Pathostain ABC-POD(M) Kit (Wako, Osaka, Japan) and diaminobenzidine tetrahydrochloride. Fluorescence intensity of three different brain slices stained with BF-227 was analyzed by defining regions of interest (ROI) and measuring the intensity of fluorescence within gray and white matter using Lumina Vision software (Mitani, Fukui, Japan). Ratios of gray matter ROI to white matter ROI were calculated as an indicator of stainability and statistical comparisons were performed using ANOVA and Scheffe post-hoc tests.

Labeling of amyloid deposits in Aβ-injected rat model

Aβ1–40 (Peptide Institute) was dissolved at 500 μmol/L in 50 mmol/L potassium phosphate buffer and incubated at 37°C for 4 days. An Aβ-injected rat model was created as described previously.[10] Briefly, Wistar rats (male, 200–250 g, SLC, Shizuoka, Japan) were injected with Aβ peptides unilaterally and potassium phosphate buffer contralaterally into each amygdala using a stereotaxic instrument (Model 5000, David Kopf, Tujunga, CA, USA). Injection coordinates measured from the bregma and skull surface (anteroposterior, −3.0 mm; mediolateral, ±5.0 mm; dorsoventral, −8.8 mm) were determined based on a stereotaxic atlas.[11] A volume of 1.0 μL was administered over 2 min using a microsyringe and glass cannula (tip diameter, 170–250 μm). At 3 days after injection of Aβ and vehicle, (^{18}F)BF-168 (72.8 MBq) or (^{18}F)BF-227 (58.9 MBq) were administered into the femoral vein of anesthetized rats. Rats were killed by decapitation at 180 min postinjection and the brains were removed and frozen. An OTF cryostat (Bright Instruments, Huntingdon, UK) was used to cut 30-μm thick frozen sections, which were then dried and exposed to a BAS-III imaging plate for 18 h. Autoradiographic images were obtained using a BAS2000 scanner system

(Fuji Film, Tokyo, Japan). After autoradiographic examination, the same sections were stained with thioflavin-S to confirm the presence of amyloid plaques.

Toxicity study in mice

A non-GLP (good laboratory practice) toxicity study was performed using female and male ICR mice (weight, 22–32 g). The Ethics Committee of BF Research Institute approved the protocol for these experiments. Animals were kept in a temperature-controlled environment (21.2–23.5°C) with a 12-h light–dark cycle and ad libitum access to food and water. In the acute toxicity study, animals were divided into one control group and three treated groups, with 10 animals (five males, five females) in each group. The control group received injection of vehicle alone, while each treated group received i.v. injection of BF-227 solution in doses of 0.1, 1 or 10 mg/kg. Animals were observed for 8 days after administration to identify any changes in general behavior or bodyweight. In the subacute toxicity study, animals were divided into one control group and two treated groups (2.5 and 25 μg/kg), with 10 animals (five females, five males) in each group. The control group received injection of vehicle alone and each treated group received i.v. injection of BF-227 solution for 14 days (once daily). Animals were weighed at 3, 7, 9 and 14 days after administration. At the end of the experiment, animals were sacrificed and examined at autopsy. Selected organs (brain, heart, liver, lung and kidney) were removed, weighed and examined microscopically by a pathologist.

Results

Binding characteristics of BF-227 for Aβ fibrils

In vitro binding assay indicated that BF-227 shows high binding affinity for Aβ fibrils. K_d for Aβ1–40 fibrils was 1.0 ± 1.4 nmol/L, comparable to previously reported levels for amyloid imaging agents[12] (Fig. 2). Binding ability of BF-227 to Aβ was also examined by fluorometric analysis, as BF-227 is highly fluorescent. In the mixture of BF-227 and Aβ peptides, fluorescence intensity of BF-227 increased as Aβ1–40 (Fig. 3a) and Aβ1–42 (data not shown) incubation time advanced. BF-227 fluorescence also increased in a linear manner with increasing concentrations of fibrillar Aβ1–42 (Fig. 3b) or Aβ1–40 (data not shown), but did not increase in mixture with non-fibrillar Aβ. These results suggest that degree of BF-227 binding reflects the amount of Aβ fibril formation.

Neuropathological staining in AD brain sections

Neuropathological examination using BF-227 indicated that amyloid plaques were clearly stained with BF-227

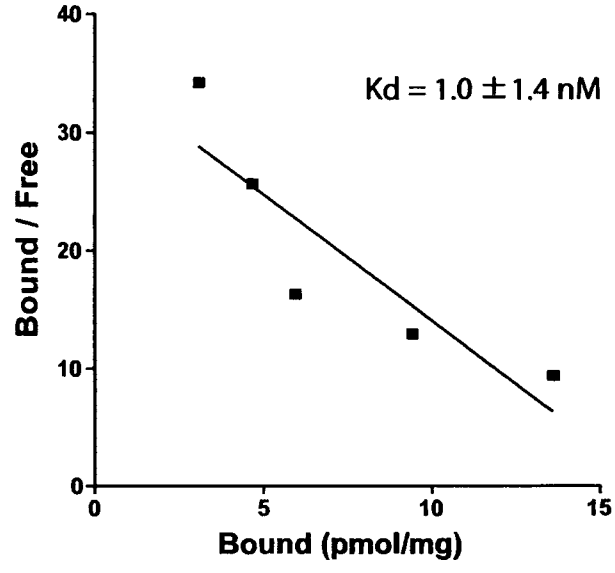

Figure 2 Scatchard plots of (^{18}F)BF-227 binding to synthetic Aβ fibrils.

in AD brain sections (Fig. 4a). In particular, cored plaques stained brightly with this compound. This staining pattern correlated well with Aβ immunostaining in adjacent sections (Fig. 4b). BF-227 staining was further compared to staining using BSB, a Congo red derivative. In contrast to clear staining of SP and NFT with BSB (Fig. 4c), BF-227 primarily stained SP, with faint staining of NFT. Preferential binding of BF-227 to SP rather than NFT represents a similar characteristic to the previously reported compound BF-145. BF-227 staining was subsequently performed in three different regions (temporal lobe, hippocampus and cerebellum) of an AD brain. In temporal (Fig. 5a) and hippocampal (Fig. 5b) sections, cored plaques stained brightly with BF-227. In contrast, no staining was evident in the cerebellum (Fig. 5c). Fluorometric measurement of these brain sections indicated that overall level of stainability in the cerebellum differed significantly from that in the temporal cortex and hippocampus (Fig. 5d), suggesting the binding specificity of this compound to AD pathology.

Intravenous administration of ^{18}F-labeled agents in Aβ-injected rat model

In vivo binding ability of (^{18}F)BF-168 and (^{18}F)BF-227 to Aβ fibrils was further evaluated by the autoradiographic experiment in the Aβ-injected rat model. In an image of the brain section at 180 min postinjection of ^{18}F-labeled agents (Fig. 6), Aβ aggregates were clearly labeled with both agents, suggesting the usefulness of these agents as *in vivo* amyloid-imaging probes. However, non-specific

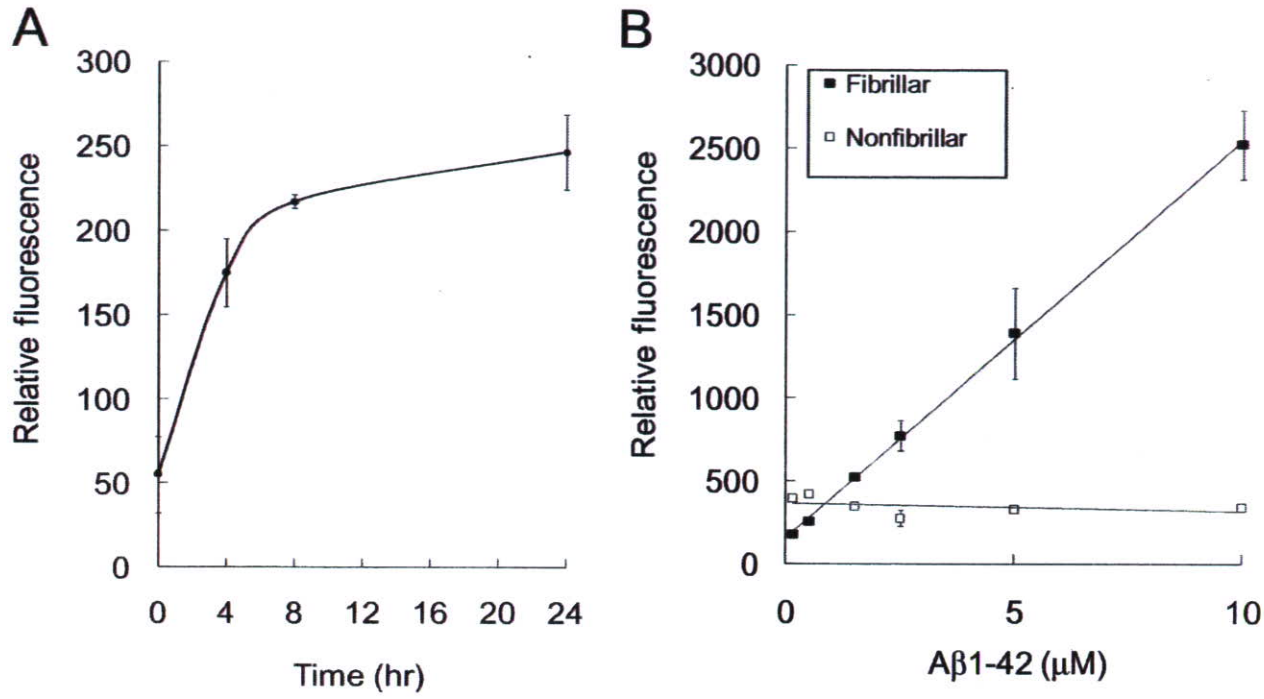

Figure 3 *In vitro* binding of BF-227 with Aβ peptides. Fluorescence intensity of BF-227 increased with Aβ incubation time (A). BF-227 fluorescence also increased linearly with concentrations of fibrillar Aβ, but did not increase in mixture with non-fibrillar Aβ (B).

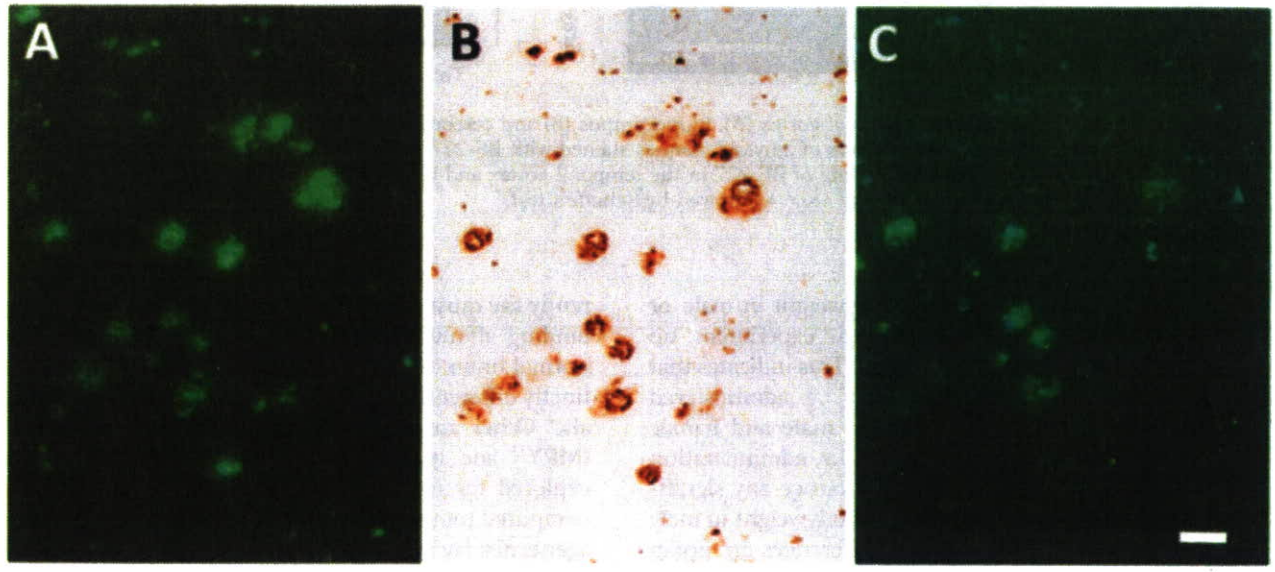

Figure 4 Neuropathological staining of Alzheimer's disease (AD) temporal brain sections by BF-227. Senile plaques are clearly stained with BF-227 (A). This staining correlates well with Aβ immunostaining in adjacent sections (B). BSB stains both senile plaques and neurofibrillary tangles (C). Bar, 200 μm.

retention of (^{18}F)BF-227 in the white matter was much less than that of (^{18}F)BF-168. This resulted in better hot spot-to-background contrast for (^{18}F)BF-227 (Fig. 6b) compared to (^{18}F)BF-168 (Fig. 6a).

Toxicity study of BF-227

In the acute toxicity study, i.v. administration of BF-227 in doses 0.1–10 mg/kg did not produce any significant